Local microvascular leakage promotes trafficking of activated neutrophils to remote organs

Charlotte Owen-Woods[1], Régis Joulia[1], Anna Barkaway[1], Loïc Rolas[1], Bin Ma[1], Astrid Fee Nottebaum[2], Kenton P. Arkill[3], Monja Stein[1], Tamara Girbl[1], Matthew Golding[1], David O. Bates[3], Dietmar Vestweber[2], Mathieu-Benoit Voisin[1] & Sussan Nourshargh[1,4*]

[1]William Harvey Research Institute, Barts and The London School of Medicine and Dentistry, Queen Mary University of London, Charterhouse Square, London, EC1M 6BQ, UK.

[2]Department of Vascular Cell Biology, Max Planck Institute for Molecular Biomedicine, Röntgenstraße 20, 48149 Münster, Germany.

[3]Division of Cancer and Stem Cells, School of Medicine, Queen's Medical Centre, University of Nottingham, Nottingham, NG7 2UH, UK

[4]Centre for Inflammation and Therapeutic Innovation, Barts and The London School of Medicine and Dentistry, Queen Mary University of London, London, EC1M 6BQ, UK.

C. Owen-Woods and R. Joulia contributed equally to this work.

A. Barkaway and L. Rolas contributed equally to this work.

M-B. Voisin and S. Nourshargh jointly supervised the work.

*Correspondence to Sussan Nourshargh: s.nourshargh@qmul.ac.uk

Abstract

Increased microvascular permeability to plasma proteins and neutrophil emigration are hallmarks of innate immunity and key features of numerous inflammatory disorders. Whilst neutrophils can promote microvascular leakage, the impact of vascular permeability on neutrophil trafficking is unknown. Here, through the application of confocal intravital microscopy, we reported that vascular permeability enhancing stimuli caused a significant frequency of neutrophil reverse transendothelial cell migration (rTEM). Furthermore, mice with a selective defect in microvascular permeability enhancement (*VEC-Y685F-ki*) showed reduced incidence of rTEM. Mechanistically, elevated vascular leakage promoted movement of interstitial chemokines into the blood stream, a response that supported abluminal-to-luminal neutrophil TEM. Through development of an in vivo cell labelling method we provided direct evidence for the systemic dissemination of rTEM neutrophils, showed them to exhibit an activated phenotype and capable of trafficking to the lungs where their presence was aligned with regions of vascular injury. Collectively, we demonstrated that increased microvascular leakage reverses the localisation of directional cues across venular walls, thus causing neutrophils engaged in diapedesis to re-enter the systemic circulation. This cascade of events offers a mechanism to explain how local tissue inflammation and vascular permeability can induce downstream pathological effects in remote organs, most notably in the lungs.

Introduction

Acute inflammation is a critically important pathophysiological response to a local stimulus (e.g. bacterial infection) characterised by local tissue infiltration of neutrophils and tissue swelling (oedema). These responses typically begin within minutes after a stimulus and collectively support the activation of essential immunoregulatory, pro-inflammatory and pro-resolution pathways required for effective host defence and tissue repair. Excessive and/or inappropriately triggered neutrophil migration and increased vascular leakage can also be the underlying cause of a vast range of acute and chronic inflammatory disorders, such as acute lung injury and rheumatoid arthritis, and are as such well-established anti-inflammatory therapeutic targets (1, 2). Central to regulation of these responses are endothelial cells (ECs) that line the inner aspect of all blood vessels and provide the principal barrier to migrating immune cells and blood-borne macromolecules. With respect to neutrophil trafficking, ECs provide critical pro-adhesive and other effector molecules that facilitate a cascade of neutrophil-EC interactions, such as neutrophil rolling, firm arrest and luminal crawling, events that are generally considered to be pre-requisite to breaching of the endothelium (3). Transendothelial cell migration (TEM) is supported by an array of EC junctional molecules, most notably PECAM-1 (CD31), members of the junctional adhesion molecule (JAM) family, VE-cadherin and others (3-5). In addition, we recently demonstrated the importance of retaining directional cues within EC junctions in facilitating luminal-to-abluminal neutrophil breaching of the endothelium (6).

With respect to vascular leakage, under basal conditions the microvascular endothelium has a low permeability to plasma proteins, and as such establishes an oncotic gradient that opposes the vascular hydrostatic pressure that would otherwise excessively move water and solutes into the tissue. This situation rapidly changes in inflammation, enabling immediate supply of plasma proteins (e.g. complement components and antibodies) to injured or infected organs through increased permeability of the vascular endothelium (7). Leakage of macromolecules in inflammation largely occurs via a paracellular route involving loosening of EC junctions (5, 7, 8) mediated via actinomyosin-based contraction of ECs and destabilisation of junctional contacts. The latter most notably involves down-regulation of the adhesive functions of VE-cadherin (5, 8) with inflammation-induced increased

vascular permeability being associated with elevated tyrosine phosphorylation of components of the VE-cadherin-catenin complex (5, 9). Of particular significance, investigations using knock-in mice expressing specific point mutations in VE-cadherin tyrosine residues (i.e. VEC-Y685F and VEC-Y713F), have categorically identified distinct molecular mechanisms in governing the passage of neutrophils and macromolecules through EC junctions (9). These findings are in line with early seminal works that definitively uncoupled in a temporal and spatial manner leukocyte extravasation from increased vascular permeability (10, 11).

Despite this, the close association of stimulated neutrophil transmigration and vascular permeability has historically attracted much attention towards their potential interplay, and indeed, it is now generally accepted that neutrophils can promote microvascular leakage in the early stages of an acute inflammatory response (12, 13). However, whether vascular permeability can regulate neutrophil migration remains poorly investigated and is contentious. To address this fundamental element of acute inflammation we used confocal intravital microscopy (IVM) to simultaneously analyse vascular leakage and neutrophil trafficking in inflamed tissues. Increased microvascular leakage did not influence the overall magnitude of neutrophil infiltration into tissues over several hours. Surprisingly however, leaky microvessels promoted a rapid and significant frequency of neutrophil reverse transendothelial cell migration (rTEM; ~20-40%) in the early phases of hyperpermeability reactions. This aberrant behaviour was caused by an immediate increase in diffusion of interstitial chemokines into the vascular lumen, a response that disrupted the correct localisation of chemotactic cues within the venular wall niche. Furthermore, through development of an in vivo cell labelling method, we provide direct evidence for the ability of rTEM neutrophils that have stemmed from an inflammatory vascular leakage site to traffic to the lungs. Functionally, rTEM neutrophils were activated, and their presence within the pulmonary vasculature was aligned with sites of vascular injury, suggesting a pathological role for this sub-set of neutrophils. Collectively by identifying that local microvascular leakage induction facilitates movement of interstitial chemokines through EC junctions and entry into the vascular lumen, we have discovered an additional mechanism for promotion of neutrophil rTEM

in vivo. Importantly, our findings directly link this cascade of events with the capacity of local hyperpermeability reactions to elicit remote organ damage.

RESULTS

Leaky venules support neutrophil reverse TEM

To directly investigate potential associations between neutrophil trafficking and microvascular permeability, inflamed mouse cremaster muscles were analysed for neutrophil breaching of EC junctions and microvascular leakage in real-time and in 3D (i.e. 4D) by confocal IVM. Briefly, the model employs *LysM-EGFP-ki* mice in conjunction with in vivo labelling of EC junctions using locally-applied non-blocking AlexaFluor-647 labelled (AF647) anti-CD31 mAb (14). Neutrophil TEM was analysed through tracking of GFP^{bright} neutrophils, and microvascular leakage was quantified by measuring interstitial accumulation of intravenously injected plasma protein tracer TRITC-dextran (MW ~75kDa) (Figure 1A and Supplemental movie 1). In initial studies we analysed inflammatory responses induced by local injections of LTB_4 and IL-1β and by a local pathophysiological insult of ischemia-reperfusion (IR) injury (all within 2-4h). Whilst these acute reactions elicited significant and comparable levels of total neutrophil infiltration into tissues within the overall test periods, as compared to control responses (Figure 1B), marked and rapid increased vascular leakage was only detected in tissues stimulated with LTB_4 and IR (Figure 1C). Of note, overtime hyperpermeability reactions were associated with uptake of tissue infiltrated dextran by perivascular cells (Figure 1A) but these regions were excluded from the image analysis process.

Most importantly, in contrast to the normal neutrophil TEM observed in IL-1β-stimulated tissues (i.e. neutrophils breaching EC junctions in a luminal-to-abluminal direction and without pause; Figure 1D and Supplemental movie S2), inflammatory reactions that increased vascular leakage were associated with the occurrence of neutrophil reverse TEM (rTEM) (Supplemental movie S3). Specifically, in LTB_4- and IR-stimulated tissues, and in line with our previous reports (14, 15), a significant proportion of neutrophils that initiated TEM by extending protrusions through EC junctions rapidly retracted their cell body, exhibited reverse motility through EC junctions, and ultimately returned back into the blood circulation (Figure 1D). This mode of neutrophil TEM accounted for ~20-40% of all TEM events driven by LTB_4 and IR but was rarely seen in IL-1β-stimulated tissues (<5%)

(Figure 1E). Using the IR reaction to analyse the onset of this phenomenon we noted that ~62% of the rTEM events occurred within the first 10min of the reperfusion phase (Figure 1F). In contrast, normal neutrophil TEM, as indicated via neutrophil accumulation in the perivascular tissue, was more sustained and continued to develop over the 2h reperfusion period analysed (data not shown). Of significance, whilst a close temporal association was observed between dextran leakage and frequency of neutrophil rTEM, the former exhibited an earlier onset (i.e. within less than 5min post reperfusion, Figure 1F). This raised the possibility that increased EC permeability can influence the directionality of neutrophil TEM, prompting us to investigate the impact of vascular leakage enhancing stimuli, histamine and VEGF-A_{164} (VEGF) on rTEM.

In agreement with previously published reports (16, 17), topical application of histamine to exteriorised cremaster muscles promoted neutrophil rolling but failed to induce neutrophil firm arrest or transmigration (Supplemental Figure 1A-C). Similarly, topical application of histamine to exteriorised IL-1β-stimulated cremaster muscles caused no significant increase in neutrophil adhesion or transmigration beyond that seen with IL-1β alone (Supplemental Figure 1D and Figure 2A). As anticipated, topical histamine induced a marked vascular leakage response in IL-1β-treated tissues as compared to tissues treated with just IL-1β or PBS (Figures 2B, C and Supplemental movie S4), however, most intriguingly, it promoted a significant frequency of neutrophil rTEM events (~20%; Figure 2D and Supplemental movie 4). Similarly, whilst i.v. VEGF induced a notable vascular leakage response in mice treated with local IL-1β (Supplemental Figure 1E) without impacting total neutrophil infiltration (Supplemental Figure 1F), it caused a dramatic increase in frequency of neutrophil rTEM (~25%; Figure 2D). Furthermore, in animals treated with IL-1β+histamine, maximal neutrophil rTEM was again detected rapidly post topical application of histamine (~80% within 20min), in line with the rapid stimulated vascular leakage (Figure 2E). Collectively, the present findings demonstrate a previously unappreciated link between induction of vascular leakage and aberrant neutrophil TEM with the induction of leakage emphatically impacting the directional migration of neutrophils through EC junctions.

Genetic defect in microvascular leakage suppresses neutrophil reverse TEM

To further investigate the causal link between increased microvascular leakage and disrupted neutrophil TEM, we took advantage of a knock-in mouse model that expresses a Y685F mutant of VE-cadherin (*VEC-Y685F*) and shows reduced vascular leakage but normal neutrophil extravasation (9). Knock-in mice expressing wild-type (WT) VE-cadherin (*VEC-WT*) were used as controls. To facilitate simultaneous quantification of neutrophil TEM dynamics and vascular leakage, chimeric mice were generated through adoptive transfer of bone-marrow from *LysM-EGFP-ki* donor mice into irradiated *VEC-WT* and *VEC-Y685F* recipients (Figure 3A). Using our model of local IL-1β+histamine, *VEC-Y685F* chimeric mice showed reduced (~26%) interstitial dextran accumulation (Figure 3B and C) with no significant change in total neutrophil extravasation over 2h (Figure 3D), as compared to responses detected in chimeric *VEC-WT* controls. These results are in line with the findings of Wessel and colleagues using the Miles assay in which 36% suppression of histamine-induced vascular leakage was detected in the dorsal skin of *VEC-Y685F* mice (9). Of note, in agreement with our previous results (Figure 2D), IL-1β+histamine caused a substantial frequency of neutrophil rTEM (~22%; Figure 3E) in *VEC-WT* chimeric mice. However, mice harbouring the mutant form of VE-cadherin exhibited a significantly reduced frequency of this response (down to ~10%), culminating in ~55% inhibition of rTEM as compared to *VEC-WT* mice (Figure 3E). Together, our results provide compelling evidence for the ability of increased vascular leakage to disrupt luminal-to-abluminal motility of neutrophils through EC junctions resulting in neutrophil reverse TEM back into the vascular lumen.

Microvascular leakage promotes trafficking of interstitial chemokines into the blood stream

We next explored the mechanism through which vascular leakage induction promotes disrupted directionality of neutrophil TEM. Since our earlier works identified reduced EC junctional expression of JAM-C as a driver of incomplete and reverse modes of neutrophil TEM (14, 15), this possibility was evaluated in the context of vascular leakage. However, local histamine, IL-1β, or the combination of

both mediators had no impact on expression of EC JAM-C (Supplemental Figure 2). In considering alternative mechanisms, we hypothesised that elevated microvascular permeability may alter the local chemotactic gradient across venular walls. To explore this notion, since IL-1β is an effective inducer of a potent neutrophil chemokine CXCL1 (18, 19), we sought to investigate the impact of increased vascular leakage on generation and localisation of CXCL1 in IL-1β-stimulated tissues.

IL-1β-stimulation of WT cremaster muscles led to a robust increase in tissue and plasma CXCL1, as compared to PBS-treated mice (Figure 4A-D). Whilst locally injected histamine or i.v. VEGF had no significant effect on IL-1β-induced tissue levels of CXCL1, they elevated the associated plasma levels of CXCL1 (Figure 4A-D). Of note, the vasoactive agents on their own did not induce either tissue or plasma CXCL1 (Figure 4A-D). Similarly, as found with IL-1β, TNF stimulation of cremaster muscles increased tissue and plasma CXCL1, with the latter being further elevated after local administration of histamine (Figure 4A and B). In addition, increased tissue and plasma CXCL1 were detected in mice subjected to the hyperpermeability-inducing reaction of cremasteric IR injury (Supplemental Figure 3). These results imply that vascular permeability enhancing stimuli can promote the trafficking of endogenously generated CXCL1 from the tissue into the blood stream. To directly investigate this possibility, we asked a general but fundamental question: can an extravascular protein, comparable to the size of a chemokine (~8kDa), traffic into the blood stream through hyperpermeable leaky microvessels? To address this, we examined by confocal IVM the localisation of topically-applied small molecular weight (10kDa) AF488-dextran in control and histamine-treated IL-1β-stimulated cremaster muscles. Here, vascular leakage was simultaneously quantified using i.v. injected high molecular weight (75kDa) TRITC-dextran. Superfusion of exteriorised cremaster muscles with 10kDa-AF488-dextran (for 10min) led to its rapid and sustained accumulation in the extravascular space surrounding blood vessels (Figure 4E and F and Supplemental movie 5). Topical application of histamine caused immediate leakage of blood-circulating 75kDa-TRITC-dextran into the interstitium (Figure 4E and G and Supplemental movie 5), confirming induction of vascular leakage. Importantly, this effect was associated with rapid (<5min) disappearance of the 10kDa-AF488-dextran signal from the perivascular space, as compared to tissues treated with topical vehicle (Figure 4E, F and G).

Furthermore, in mice treated with topical histamine, a significant level of 10kDa-AF488-dextran was detected in plasma (Figure 4H).

Collectively these results demonstrate that under conditions of enhanced vascular permeability, a small MW protein can diffuse from the interstitium into the blood stream against an advective flow in the opposite direction. As seemingly unexpected, further validation of these experimental findings were sought through mathematical modelling. Briefly, as the molecular flux across the vessel wall is determined by a combination of diffusive and advective transport, for a small MW protein in the extravascular compartment (e.g. 10kDa dextran or a chemokine) to enter the blood circulation, the diffusive flux from tissue to blood must be high enough to overcome the opposing advective flux (Figure 4I). This ratio is defined by the Péclet number (*Pe*) (Figure 4I). If the *Pe* is substantively less than 1, then there can be diffusion against an advective flow of fluid. If the *Pe* is >1 then diffusion cannot effectively oppose filtration – in other words for a molecule to diffuse against a flow of fluid *Pe* needs to be <1. Using previously published values for the hydraulic conductivity properties of ECs, and known diffusion coefficients, the *Pe* number for a 10kDa dextran in cremaster muscle microvessels is calculated to be ~0.8 under normal conditions (Supplemental Figure 4). Such a scenario would allow some diffusion of interstitial protein into the vascular lumen, in line with our experimental data (Figure 4H). However, under conditions of increased vascular permeability (e.g. as induced by local histamine) this falls substantially to values at which diffusion dominates advective flux (i.e. *Pe*<0.3; Figure 4I and Supplemental Figure 4). This modelling of the molecular flux across cremasteric venular walls supports our experimental data and provides additional endorsement for the concept that vascular hyperpermeability can facilitate the trafficking of extravascular small molecules into the vascular lumen.

We next directly assessed the capacity of an interstitial chemokine to engage with EC junctions and to leak from the tissue into the bloodstream post vascular permeability induction. For this purpose, we analysed the localisation of human CXCL8 (hCXCL8) in relation to ECs, when locally applied to IL-1β-stimulated cremaster muscles, in the presence or absence of histamine. Although in control tissues the chemokine was modestly aligned with the endothelium, this was significantly elevated post

local application of histamine, most notably in relation to EC junctions (Figure 5A and B). Furthermore, whilst locally injected hCXCL8 could be detected in plasma of mice treated with IL-1β only, this response was significantly increased (~42%) in mice treated with IL-1β+histamine (Figure 5C). A similar increase in plasma levels of locally injected hCXCL8 was noted in mice treated with IL-1β+VEGF as compared to animals treated with IL-1β+vehicle (Supplemental Figure 5). Furthermore, VEC-Y685F mutant mice that exhibit a defect in vascular permeability induction (9) (Figure 3B and C), showed reduced plasma levels of hCXCL8 as compared to levels detected in control VEC-WT animals (Figure 5D). The link between vascular permeability induction and tissue to blood chemokine movement was further investigated through the use of blocking anti-VE-PTP and anti-VE-cadherin antibodies. Specifically, an anti-VE-PTP Ab that inhibits vascular permeability induction through activation of Tie-2 (20, 21), (i) significantly suppressed histamine-induced vascular leakage in the mouse cremaster muscle (Supplemental Figure 6A), and, (ii) significantly reduced plasma levels of locally administered hCXCL8 in mice treated with IL-1β+histamine, as compared to control Ab treated-mice (Figure 5E). Animals treated with the anti-VE-PTP Ab also showed reduced plasma levels of endogenously generated CXCL1 as compared to levels detected in control Ab-treated mice (Supplemental Figure 6B). In contrast to the inhibitory effects of the anti-VE-PTP Ab, a blocking anti-VE-cadherin mAb (clone BV13) (22) that promoted vascular leakage induction in the mouse cremaster muscle (Supplemental Figure 6C and D), enhanced plasma levels of locally administered hCXCL8 as compared to levels detected in control mAb (anti-CD31)-treated mice (Figure 5F).

Together, through experimental and mathematical modelling, we provide compelling evidence to show that the loosening of EC junctions during increased vascular permeability can promote the mobilisation of small MW proteins from the interstitial tissue to the blood stream and thus influence the compartmentalisation of extravascular chemokines.

Luminal CXCL1 promotes neutrophil reverse TEM

We next investigated the functional impact of increased plasma CXCL1 on neutrophil TEM. For this purpose, 2h post stimulation of cremaster muscles with IL-1β, *LysM-EGFP-ki* mice were injected i.v. with a blocking anti-CXCL1 mAb prior to topical application of histamine. Whilst at the dose employed, i.v. administration of the anti-CXCL1 mAb had no impact on plasma protein leakage or total neutrophil extravasation (Figure 6A and B), this intervention significantly reduced the frequency of neutrophil rTEM events (~60% inhibition) as compared to control Ab-injected mice (Figure 6C). Similarly, systemic CXCL1 blockade had no impact on total neutrophil extravasation in cremaster muscles subjected to IR insult (Figure 6D) but suppressed neutrophil rTEM in this permeability-enhancing reaction (~60% inhibition; Figure 6E). Suggesting that luminal CXCL1 can drive neutrophil rTEM, this was categorically investigated through i.v. injection of exogenous CXCL1 in *LysM-EGFP-ki* mice stimulated locally with IL-1β (2h). Within this protocol, i.v. CXCL1 promoted a substantial frequency of neutrophil rTEM through cremasteric venules (~30%; Figure 6F), whereas as noted previously (Figure 1E), local IL-1β on its own did not cause neutrophil rTEM (Figure 6F). Collectively, the present results unequivocally demonstrate that vascular CXCL1 can drive neutrophil TEM towards the luminal aspect of the endothelium.

Development of a cell labelling strategy for tracking of neutrophil rTEM in vivo

Aiming to gain insight into the fate, phenotype and pathophysiological relevance of rTEM neutrophils stemming from a local hyperpermeability inflammatory site, we established a method for tracking of these cells. Previous studies employing zebrafish and murine models of tissue injury have utilised genetically encoded photolabelling protocols to track reverse migrating neutrophils from within injured interstitial tissues back into the vascular lumen and into distal organs (23-25). However, as the neutrophil reverse migration phenomenon noted in the present study is restricted to breaching of the endothelium only, photoconverting and photoactivation of neutrophils confined within tight EC junctions or the thin sub-EC space (<3μm wide) renders such genetic strategies inappropriate for exclusive delineation of rTEM cells (e.g. preliminary works with transgenic mice expressing the Kaede

photoconvertible fluorescence protein tracked <10 rTEM neutrophils/inflamed tissue; data not shown). Hence, as part of the present study we have developed a labelling method that crisply delineates neutrophils that reverse migrate within EC junctions and re-enter the vascular lumen (Figure 7A). The method takes advantage of the strong affinity of streptavidin for biotin and our observation that locally applied streptavidin is retained within the cremaster muscle tissue and does not move into the systemic circulation, even under conditions of increased vascular permeability (Supplemental Figure 7A). Initial experiments applied this labelling method to staining of neutrophils in IL-1β-stimulated tissues. Briefly, after local application of IL-1β (1.5h), *LysM-EGFP-ki* mice were injected i.v. with biotinylated anti-Ly6G mAb, a step that as anticipated selectively labelled >99% of all circulating neutrophils (Supplemental Figure 7B). Thirty minutes later, cremaster muscles were surgically exteriorised and tissues were topically superfused with AF647-streptavidin. Analysis of tissues by confocal microscopy showed that with this protocol luminal neutrophils were GFP^+ but $streptavidin^-$, whilst neutrophils in the sub-EC space and in the interstitial tissue were clearly positive for both GFP and streptavidin (Figure 7B). We next sought to investigate the ability of this labelling method to track rTEM neutrophils during the hyperpermeability IL-1β+histamine reaction where histamine and AF647-streptavidin were simultaneously superfused onto surgically exteriorised tissues. Here, intriguingly we noted that in neutrophils exhibiting TEM, leading protrusions in the sub-EC space rapidly became intensely $streptavidin^+$ (Figure 7C), resulting in effective labelling of all neutrophils that partially or fully breached the endothelium. This included cells that completely breached the venular wall and entered the surrounding interstitial tissue as well as cells that reverse migrated from within EC junctions or the sub-EC space back into the vascular lumen (Figure 7A-D). Similar results were obtained when AF647-streptavidin was injected locally into cremaster muscles (400ng for 2h) as opposed to being topically superfused (Supplemental Figure 7C and D). Of importance, unlabelled mice and mice subjected to the biotin-streptavidin labelling strategy exhibited similar levels of neutrophil migration into tissues and neutrophil rTEM (Supplemental Figure 8A and B as compared to Figures 2A and D) as well as similar neutrophil migration velocity within EC junctions and the interstitial tissue (Supplemental Figure 8C and D).

Thus, we have established a cell labelling technique for direct tracking of neutrophils that exhibit reverse TEM in vivo. This methodological advancement enables definitive explorations into the phenotype and fate of rTEM neutrophils.

Reverse TEM neutrophils disseminate into the systemic and pulmonary circulation and exhibit an activated phenotype

Exploiting our labelling method, we next investigated the distribution of rTEM neutrophils stemming from local hyperpermeability sites. Since our confocal IVM studies showed rTEM neutrophils to re-enter the vascular lumen and rapidly detach from the luminal aspect of the endothelium (Supplemental Video 6), we initially sought to detect these cells in the systemic circulation. For this purpose, using mice subjected to cremasteric stimulation with IL-1β, blood samples were taken two hours post local administration of histamine or vehicle in conjunction with the new biotin-streptavidin labelling protocol. Flow cytometry analysis of samples from IL-1β-treated mice showed very low levels of streptavidin$^+$ circulating blood neutrophils (~0.1%, corresponding to a total of ~800 streptavidin$^+$ neutrophils/ml of blood); this number was significantly increased in blood samples of mice locally stimulated with IL-1β+histamine (~0.4%, corresponding to ~2,800 streptavidin$^+$ neutrophils/ml of blood) (Figure 8A and B). Aligned with the substantive frequency of neutrophil rTEM seen in the corresponding reactions (see Figure 2D), these results strongly indicated the presence of rTEM neutrophils in the systemic circulation. Focussing on the hyperpermeability reaction to IL-1β+histamine, we next explored the phenotype of streptavidin$^+$ neutrophils as compared to streptavidin$^-$ cells. Streptavidin$^+$ blood neutrophils exhibited no significant change in expressions of L-selectin (CD62L), β1 integrins, ICAM-2, neutrophil elastase (NE) or CXCR4 but showed significantly increased expression of CD11b, and a low but significant increase in expression of ICAM-1 (Supplemental Figure 9A and Figure 8C). Based on such an activated phenotype, and as guided by our previous works (14, 15), we hypothesised that streptavidin$^+$ rTEM neutrophils may be additionally retained within the pulmonary

vasculature. To address this possibility, we analysed the percentage and phenotype of streptavidin$^+$ neutrophils in pulmonary vasculature washouts of mice subjected to local cremaster muscle stimulations with PBS, histamine, IL-1β or IL-1β+histamine (2h) and biotin-streptavidin labelling. Whilst animals treated locally with PBS, histamine or IL-1β showed similar levels of streptavidin$^+$ neutrophils (~0.2%), mice stimulated with IL-1β followed by histamine for 2h showed an enrichment of streptavidin$^+$ neutrophils in the pulmonary vasculature (~0.8%) (Figure 8D and E). Increasing the local stimulation period with histamine to 4h resulted in a similar level of streptavidin$^+$ neutrophils in blood (~0.42%) but led to a reduced and non-significant level in the pulmonary vasculature (~0.2%) (Supplemental Figure 9B and C). Interestingly, in mice treated locally with IL-1β followed by 4h stimulation with histamine, but not 2h, a significant level of streptavidin$^+$ neutrophils was detected in the bone marrow (Supplemental Figure 9D, E, F and G). Together these results suggest that the retaining of rTEM neutrophils in the lungs is transient and that this subset of cells eventually migrate to the bone marrow. Furthermore, as compared to streptavidin$^-$ cells, streptavidin$^+$ pulmonary vascular neutrophils showed no significant change in expressions of L-selectin and ICAM-2 but exhibited a significant increase in expressions of β1 integrins, CD11b, ICAM-1, NE and CXCR4 (Figure 8F and G). The latter is in line with the observed trafficking of the streptavidin$^+$ cells to the bone marrow. Of note, in IL-1β+histamine-treated mice subjected to our labelling protocol, streptavidin$^-$ neutrophils in both blood and pulmonary vascular washout samples showed a similar phenotype to neutrophils acquired from un-labelled mice treated locally with just PBS, histamine or IL-1β alone (Supplemental Figure 10A and B). This crucial set of data precludes the possibility that in IL-1β+histamine-treated mice circulating soluble factors determine the phenotype of the streptavidin$^+$ cells. Additionally, these results suggest that the streptavidin$^+$ rTEM neutrophils have no impact on the phenotype of streptavidin$^-$ neutrophils.

Together, we provide evidence for the ability of rTEM neutrophils stemming from a local hyperpermeability site to re-enter the systemic circulation and to traffic to lungs, where they exhibit an activated pro-adhesive phenotype, before returning to the bone marrow.

Disseminated rTEM neutrophils localise to sites of vascular leakage in lungs

We have previously shown an association between rTEM neutrophils stemming from local inflammatory sites characterised by reduced junctional expression of EC JAM-C and remote organ injury (14, 15). We therefore hypothesised that neutrophil rTEM driven by local hyperpermeability could similarly cause distant organ damage. To investigate this notion, pulmonary vascular leakage resulting from stimulation of cremaster muscles was assessed by measuring sub-EC and extravascular accumulation of intravenously administered fluorescent microspheres (26). Furthermore, to investigate if this response was associated with accumulation of rTEM neutrophils stemming from the cremaster muscle, the experiments incorporated the new biotin-streptavidin labelling protocol. Our findings showed that mice subjected to cremaster muscle stimulation with IL-1β+histamine, but neither stimulus on its own or local PBS, exhibited lung vascular leakage (Figure 9A and B). In addition, whilst all reactions tested exhibited similar levels of total neutrophil recruitment to lungs (~15 neutrophils/field of view), a significantly elevated number of streptavidin$^+$ neutrophils was detected in lungs of mice subjected to cremaster muscle local hyperpermeability (Figure 9C). Furthermore, these studies indicated a significant association between numbers of streptavidin$^+$ neutrophils and the extent of increased lung vascular permeability (Figure 9D) and a significant association between the presence of streptavidin$^+$ neutrophils and sites of pulmonary vascular leakage (Figure 9E and F). Collectively, the findings demonstrate that a local hyperpermeability reaction can promote distal organ injury by recruitment of rTEM neutrophils (Figure 10).

DISCUSSION

Enhanced microvascular leakage and neutrophil trafficking are pivotal features of an acute inflammatory response. Importantly, the molecular basis of these events are distinct (9) and there is ample evidence to show that neutrophil extravasation in vivo *per se* is not sufficient for increased microvascular leakage (present study and (10, 11)). None-the-less, neutrophils, most notably when stimulated to adhere by certain chemoattractant mediators (27, 28), can secrete a range of pro-permeability factors (e.g. VEGF, LTA_4, HBP, TNF) (12, 13, 29-31). Here we report for the first time that increased vascular permeability can also impact neutrophil trafficking by reversing the directional luminal-to-abluminal migration of neutrophils through the endothelium. Mechanistically, this was governed by disrupted localisation of tissue chemokines as induced by the movement of chemokines into the vascular lumen through leaky venular walls. Crucially, we demonstrate that neutrophils stemming from hyperpermeability sites re-enter the systemic circulation, exhibit an activated phenotype and traffic to the lungs where they are present at sites of vascular injury. Collectively, through identifying a previously unreported link between two fundamental components of inflammation, our findings extend current understanding of pathological inflammation and suggest that targeting local microvascular permeability may provide an effective means of suppressing neutrophil-mediated remote organ damage.

Intrigued by the lack of investigations into the potential impact of increased vascular permeability on neutrophil trafficking, we applied high resolution confocal IVM for simultaneous analysis of these phenomena. Our findings revealed that induction of vascular leakage does not grossly alter total tissue infiltration of neutrophils over several hours. However, unexpectedly, augmented vascular leakage rapidly promotes a significant frequency of neutrophils that have initiated TEM to exhibit retrograde motility within EC junctions and eventually re-enter the blood circulation. Increased microvascular permeability consistently preceded the occurrence of this aberrant TEM response, suggesting a causal link. Direct evidence for this notion was acquired through the use of knock-in mice expressing a Y685F mutant of VE-cadherin with selective impaired vascular permeability induction (9) that showed reduced disrupted neutrophil TEM. Neutrophil reverse migration within EC

junctions, termed “reverse TEM”, has previously been described by our group in relation to multiple inflammatory scenarios in the murine microcirculation (6, 14, 15). This response, which was first described in vitro for human neutrophils (32) is, however, one of a number of neutrophil reverse migration modes that to date have been reported in numerous contexts, experimental models and inflammatory conditions (23-25, 33-35). The wide-ranging profiles and potential implications of neutrophil retrograde migration begs the need for further explorations of this enigmatic response in terms of its mechanisms and consequences.

In addressing the mechanisms that drive neutrophil rTEM, our previous works identified neutrophil elastase-mediated cleavage of EC junctional JAM-C as a trigger of this cellular response (14, 15). Together with in vitro studies of monocyte TEM (36), these findings indicated a need for EC JAM-C as a regulator of one-way leukocyte trafficking through EC junctions, though the precise molecular basis of JAM-C-mediated luminal-to-abluminal neutrophil motility remains unclear. Of note however, directly-acting vascular permeability enhancing agents (histamine and VEGF) that effectively instigated neutrophil rTEM in IL-1β-stimulated tissues, had no impact on JAM-C expression. As an alternative mechanism, and based on recent findings showing the significance of compartmentalised directional cues in promoting neutrophil diapedesis (6), we hypothesised that increased vascular permeability may disrupt the correct positioning of chemotactic signals within the venular wall niche. Focussing on CXCL1, a potent neutrophil chemoattractant abundantly generated within our acute inflammatory models, elevated plasma levels of this chemokine were noted in all hyperpermeability reactions tested. Intriguingly, these results suggested that vascular leakage can prompt the diffusion of endogenously generated CXCL1 from the tissue and/or the venular wall into the vascular lumen. Support for this notion was acquired through tracking of topically applied 10kDa dextran in histamine-stimulated tissues by confocal IVM and such an event was predicted by mathematical modelling. Briefly, whilst under normal homeostatic conditions, intact EC contacts provide a significant barrier to movement of molecules into tissues, this situation changes in inflammation. When vascular permeability is increased, EC junctional contacts loosen and although this supports increased hydraulic flux, it also causes a decrease in hydraulic velocity. Such a scenario can facilitate diffusion

of a small molecule (e.g. a chemokine) from the tissue back into the blood stream as shown here both experimentally and mathematically. This hypothesis was conclusively validated through assessing the interstitial to vascular lumen distribution of exogenous hCXCL8 following specific genetic or pharmacological modulations of vascular permeability induction. Collectively, the findings reveal that hyperpermeability inflammatory conditions can promote reverse diffusion of chemokines from the tissue to the vascular lumen, a phenomenon that can disrupt the directional motility of neutrophils through EC junctions. The latter was definitively illustrated in experiments where systemic blockade of CXCL1 prevented neutrophil rTEM in hyperpermeability reactions, and conversely, intravenous exogenous CXCL1 promoted neutrophil rTEM.

The sequence of molecular and cellular events that guide neutrophils from the vascular lumen to the interstitial tissue is well established and described by the leukocyte adhesion cascade (3). Here, it is considered that chemokines immobilised on the luminal aspect of blood vessels trigger the local arrest of neutrophils (3) with sequential, compartmentalised and locally presented chemotactic cues within venular walls promoting luminal-to-abluminal diapedesis (6). Whilst glycosaminoglycans (GAGs) are considered to provide the principal mode of retaining chemokines on the luminal aspect of blood vessels, the retention of chemokines within EC junctions is likely mediated by binding to the atypical chemokine receptor ACKR1 that is enriched at these sites (6, 37). Together, due to their pivotal role in localisation, retention and/or transport of chemokines, ACKR1 and GAGs are key molecular players in supporting leukocyte trafficking (38, 39). In contrast to these physiological regulatory modes, increased vascular permeability appears to account for excessive EC junctional motility and resultant entry of chemokines into the blood stream. As such, local hyperpermeability disrupts the correct spatiotemporal presentation of chemotactic cues within venular walls, and in doing so, disrupts a phenomenon that is critical for efficient and unidirectional luminal-to-abluminal migration of neutrophils (6).

Although migration away from sites of inflammation and injury is now an established neutrophil behaviour (34), it is highly plausible that the implications of this response are different in diverse contexts and in varied experimental models. Most notably, neutrophil retrograde motility within

interstitial tissues away from sites of sterile injury, and in some cases re-entry into the blood circulation, is proposed as a component of inflammation resolution (24, 33, 40, 41). For example, Wang and colleagues reported that neutrophils recruited to a murine thermal hepatic injury model contributed to revascularisation of injured tissues and subsequently left the injured site by re-entering the local vasculature (24). Using an elegant mouse model that selectively expressed a photoactivatable GFP in neutrophils, the authors could track ~10% of the tissue infiltrated neutrophils, a procedure that enabled a small number of cells to be tracked to the lungs and a higher number to the bone marrow. Phenotypic analysis of photoactivated neutrophils in these organs indicated increased expression of CXCR4. Based on the latter, it was concluded that neutrophil migration away from injured tissues is a physiological process that may regulate deactivation and/or reprogramming of neutrophils in the lungs before they are recruited to the bone marrow via CXCR4 for eventual clearance by apoptosis (24). The neutrophil reverse motility response reported in our study is distinctly different from that analysed by Wang and colleagues in that it is restricted to EC junctions and the sub-EC space and collectively describes the re-entry of transmigrating neutrophils back into the vascular compartment prior to the cells fully exiting the venular wall. Whilst we have previously associated this response with remote organ damage (14, 15), our earlier works did not provide direct evidence for rTEM neutrophils trafficking to secondary organs. To address this vital point, here we have developed an in vivo cell-labelling method that precisely and efficiently distinguishes luminal neutrophils from all cells that breach EC junctions and hence tags all TEM and rTEM neutrophils stemming from the tissue under investigation. As such, a notable strength of our method is that it enables analysis of the full sub-population of rTEM neutrophils migrating away from an inflammatory site in terms of their fate, phenotype and pathophysiological relevance.

The application of our tracking method indicated dissemination of labelled rTEM neutrophils from a local hyperpermeability site to the systemic circulation where they showed an activated phenotype (increased CD11b and ICAM-1). In the same animals, labelled rTEM neutrophils were detected at significantly elevated levels in the pulmonary vasculature with an even greater activation state, exhibiting further increased expressions of CD11b and ICAM-1, as well as β1 integrins and NE. The

latter is highly indicative of degranulation contributing to some of the noted rTEM neutrophil phenotype and indeed neutrophils are known to express preformed stores of β2 and β1 integrins that can be mobilised to the cell surface during TEM (42). Certainly, there is ample evidence showing that engagement of neutrophils with EC junctional molecules can trigger signalling and transcriptional events within migrating leukocytes (42), suggesting that rTEM and tissue infiltrated neutrophils may exhibit similar phenotypes. In line with this notion, whilst increased expression of ICAM-1 on neutrophils is a slow and transcriptionally regulated process (43), both tissue infiltrated and rTEM neutrophils can exhibit an ICAM-1^{hi} phenotype (14, 32, 43). Of importance however, although increased expressions of integrins, other granular proteins and ICAM-1 on tissue infiltrated neutrophils collectively support effective breaching of venular walls, interstitial tissue migration and pathogen clearance (42-46), such a phenotype on neutrophils that re-enter the blood circulation could be highly detrimental to the host. In line with this notion, we detected a direct association between labelled rTEM neutrophils and lung injury, results that support the paradigm that rTEM neutrophils are a sub-set of activated neutrophils that can contribute to turning a local inflammatory response into a systemic phenomenon. The precise mechanism through which rTEM neutrophils exert tissue damage remains to be elucidated. However, the strong association of NE with the pathogenesis of numerous acute and chronic lung disorders (47) suggest increased expression of this serine protease on rTEM neutrophils could be a significant factor. Furthermore, elevated expression of integrins, together with the ICAM-1^{hi} phenotype, may support increased aggregation and activation of rTEM neutrophils (e.g. degranulation and ROS generation) within small blood vessels of remote organs. Of direct relevance to this notion, we have previously shown that neutrophil ICAM-1 expression correlates with increased ROS generation (43). Additionally, pulmonary vasculature (but not blood) rTEM neutrophils showed increased expression of CXCR4, and rTEM neutrophils could be detected in the bone marrow four hours post their induction. These results collectively support the belief that neutrophils are retained within the lung vasculature in a transient manner during which they may be reprogrammed for homing to the bone marrow (24). The difference between our findings and those of other groups in terms of linking neutrophil rTEM to distant organ damage could lie in the nature of the reactions investigated, the type of retrograde migration being analysed and phenotype of the neutrophils stemming from the

primary inflammatory site. Significant to our findings, acute lung injury is a life-threatening consequence of numerous local hyperpermeability-inducing conditions such as trauma, and pathologies induced by IR injury (48, 49). Thus, we propose that activated rTEM neutrophils stemming from local hyperpermeability inflammatory sites could provide a detrimental “cellular” link between primary and secondary sites of pathological inflammation.

In summary, the present results offer a causal link between increased local microvascular leakage and neutrophil rTEM, an axis associated with development of remote organ damage. Fundamental to this cascade of events is the discovery that increased vascular leakage can induce rapid translocation of chemokines from the interstitium into the systemic circulation against hydraulic flow, resulting in disrupted directional gradient across the venular wall. This response in turn drives the re-entry of an activated sub-set of neutrophils back into the vascular lumen that can then contribute to development of lung injury. Collectively, our findings suggest that targeting excessive local microvascular permeability maybe a plausible therapeutic strategy for protecting the host from secondary organ damage. Furthermore, our results could have implications for tumour cell intravasation and dissemination from primary sites of tumour growth that are characterised by leakiness of their blood vessels.

METHODS

Antibodies

The following were obtained commercially: Anti-CD31 (390), PE-anti-CXCR4 (2B11), anti-VE-cadherin (BV13), control anti-rabbit, anti-VE-cadherin (eBioBV14) mAbs from ThermoFisher (Waltham, USA); PB-anti-Gr-1 (RB6-8C5), BV605-anti-CD62L (MEL-14), BV711-anti-CD11b (M1/70), AF488-anti-CD115 (AFS98), AF488-anti-CD102 (3C4 MIC2/4), PE/Dazzle594-anti-CD54 (YN1/1.7.4), PE/Cy7-anti-CD29 (HMβ1-1), APC-Cy7-anti-CD115 (AFS98), Biotin-anti-Ly-6G (1A8) mAbs from Biolegend (Cambridge, UK); Blocking anti-CXCL1 (48415) from R&D Systems (Abingdon, UK); Rabbit anti-human CXCL8 (NBP2-33819) from NOVUS (Abingdon, UK); Anti-NE (ab68672) from Abcam (Cambridge, UK); Anti-αSMA (1A4), anti-CD31 (2H8) from Sigma-Aldrich (Poole, UK). Rabbit polyclonal anti-VE-PTP was generated as described (50). The following were gifts: Rabbit polyclonal anti-JAM-C (clone H33; Dr Michel Aurrand-Lions, INSERM, CRCM, France) and anti-MRP14 mAb (Dr Nancy Hogg, The Francis Crick Institute, UK).

Animals

Male WT C57BL/6 (Charles River, UK) and *LysM-EGFP-ki* (51) mice (8-12 weeks old) were used for all studies. *VEC-Y685F-ki* mutant mice that exhibit a single point mutation in VE-Cadherin were generated as previously described (9).

Generation of chimeric mice

VEC-WT and *VEC-Y685F* mice were lethally irradiated with 1 dose of 9 Gy over a time period of 11min and were subsequently injected i.v. with 1.5-3x10^6 bone marrow cells from *LysM-EGFP-ki* mice. Level of engraftment was evaluated 4 weeks after reconstitution and all mice showed more >99% of GFP^+ neutrophils with similar neutrophil counts.

Confocal IVM of the mouse cremaster muscle

Anaesthetised (isofluorane, 3%) male mice received an intrascrotal (i.s.) injection of fluorescently-labelled anti-CD31 mAb (4μg) and/or IL-1β (50ng, R&D Systems, UK), LTB_4 (300ng, Cambridge Bioscience, UK) to label vessels within the tissue and/or induce an inflammatory response, respectively. Control animals received PBS. The cremaster muscles were then prepared for intravital imaging 2h or 30min post IL-1β or LTB_4 administrations, respectively, as described (14, 15). Topical application of histamine (30μM, Sigma-Aldrich) onto exteriorised tissues, or intravenous (i.v.) injection of VEGF (4μg/mouse, R&D Systems) was used to induce vascular leakage. Ischemia-reperfusion (IR) injury was induced as described (14, 15). In some experiments, anti-CXCL1 mAb or control IgG2a (1mg/kg) and anti-VE-PTP Ab (100-200μg) or rabbit IgG control (200μg) were injected i.v. as indicated in relevant texts. In some works, recombinant mCXCL1 (50ng, Peprotech, UK) was injected i.v. 2h post IL-1β. To visualize vascular leakage, 75kDa-TRITC-dextran (40mg/kg, Sigma-Aldrich) was injected i.v. (via tail vein cannula) 1min prior to the superfusion of histamine, in combination with i.v. injection of VEGF or during the reperfusion phase of IR-stimulated tissues. In some experiments, 10kDa-AF488-dextran (10μg/ml, ThermoFisher) was superfused 2min after i.v. injection of 75kDa-TRITC-dextran for 10min. The superfusate was then replaced by either Tyrode's solution containing histamine (30μM) or vehicle control for an additional 30min. To label rTEM neutrophils, biotinylated-anti-Ly6G mAb (2μg) was injected i.v. 1.5h after IL-1β stimulation of tissues. Following exteriorisation, the cremaster muscle was superfused with AF647-streptavidin (1μg/ml, ThermoFisher) with Tyrode's solution with or without histamine (30μM). Z-stack images of post-capillary venules (20-40μm in diameter) were captured using Leica SP5 or SP8 confocal microscopes incorporating a x20 water-dipping objective (NA 1.0), as detailed (6, 14).

Quantification of neutrophil TEM, microvascular leakage and streptavidin labelling

Still images and 4D live recordings were analysed using IMARIS software™ (Bitplane, Zurich, Switzerland). Extravascular neutrophils were defined as those that had fully transmigrated and passed through the pericyte layer, recognisable via a change in their morphology and expressed as

number of cells/mm^3 of tissue. Reverse TEM neutrophils were defined as cells that moved in an abluminal-to-luminal direction within EC junctions. Normal neutrophil TEM was classified as a response in which the cells migrated through EC junctions only in a luminal-to-abluminal direction, as previously described (14, 15). Extravascular leakage was quantified by interstitial accumulation of i.v. 75kDa-TRITC-dextran and presented as MFI of indicated time-points, measuring 6-8 regions of interest (ROI) in the interstitium (excluding areas exhibiting dextran-positive perivascular cells) and 30μm away from the vessel wall. These readings were then normalised in relation to the first two MFI readings obtained post i.v. injection of the tracer and presented as normalised MFI. Similar analysis was conducted for the quantification of tissue levels of 10kDa-AF488-dextran (MFI normalised to the first two readings post superfusion of the tracer). Interstitial neutrophil speed and fluorescence intensity of AF647-streptavidin were analysed using the spot or iso-surface functions of IMARIS software, respectively.

Bright-field IVM of the mouse cremaster muscle

Mice were injected i.s. with IL-1β (50ng) or PBS alone for 2h prior to cremaster muscle exteriorisation and prior to the superfusion of histamine (30μM) or vehicle, as described above. Leukocyte rolling, firm arrest and extravasation within 20-40μm post-capillary venules were quantified by IVM over a 1.5h period using a bright-light microscope (Axioskop FS, Carl Zeiss, UK), as detailed (44). Several vessel segments (3-5) from multiple vessels (3-5) were quantified for each animal.

Quantification of chemokine and dextran levels in tissue and plasma

Anaesthetised (isofluorane 3%) mice were subjected to cremasteric ischemia (40min) or injected i.s. with IL-1β (50ng) or TNF (300ng R&D Systems, Abingdon, UK) in 200μl PBS. Control animals received PBS only. Two hours later, animals were injected with i.s. histamine (30μM solution) or PBS (both in 200μl) or i.v. VEGF (4μg/mouse) or PBS. Cremaster muscles and plasma samples (in 50mM of EDTA) were harvested 30min later. In some experiments hCXCL8 (500ng, Peprotech) was co-injected with IL-1β (50ng) for 1h prior to the end of the in vivo test period (i.e. 2.5h). In some

experiments, mice were treated i.v. with a blocking anti-VE-PTP Ab (200μg) (20, 21) or rabbit IgG control (200μg) 30min after hCXCL8 and IL-1β injection. Other experiments involved treating the mice with a blocking anti-VE-cadherin mAb (BV13; 100μg) (22) or a control mAb (anti-CD31 mAb, clone 390; 100μg) i.s. for 3h followed by local injection of hCXCL8 for 1h prior to tissue and plasma collection. Tissues were homogenised in PBS containing 0.1% Triton X-100 and 1% Halt Protease and Phosphatase Inhibitor cocktail (ThermoFisher) and mechanically dissociated using the Precellys24 beat-beading system (Bertin Technologies, France). Levels of mCXCL1 and hCXCL8 were analysed as per the manufacturer's instructions by ELISA (R&D Systems and ThermoFisher, respectively, sensitivity: 2pg/ml). The quantity of chemokine detected in tissues was normalised to protein content as determined using a BCA assay (Thermo Fisher). Levels of 10kDa-AF488-dextran in plasma was quantified using a NOVOstar (0700) microplate reader.

Immunofluorescence staining and confocal analysis of tissues

Whole-mount cremaster muscles were analysed for expressions of hCXCL8, JAM-C, red-(580/605)-microbeads (20nm in diameter, $9.1x10^{13}$ beads; ThermoFisher Waltham, MA, USA), and AF647-streptavidin as previously published (6, 15). Briefly, surgically removed tissues were fixed in ice-cold PFA (4% in PBS) for 45min, blocked and permeabilised at room temperature for 4h in PBS containing 25% FCS and 0.5% Triton X-100, and incubated overnight (anti-hCXCL8, anti-MRP14, anti-α-SMA, anti-CD31 staining) or 72h (anti-JAM-C staining) at 4°C with primary antibodies. Immunostained tissues were imaged with an inverted Zeiss 800 confocal laser-scanning microscope. JAM-C expression within the VE-cadherin channel was quantified as previously described (14, 15). For analysis of hCXCL8 localisation, ECs, neutrophils and pericyte isosurfaces were created based on regions immunostained for CD31 ($CD31^{high}$ junctional and $CD31^{dim}$ non-junctional regions), MRP14 and α-SMA, respectively. EC body and junctional hCXCL8 expressions were quantified as MFI within these isosurfaced regions. The MFI of fluorescent beads present in the sub-endothelial space (<1μm from ECs) was quantified as a measure of cremaster muscle vascular leakage. An isosurface using the CD31 channel was generated to exclude fluorescent signal of beads inside the vascular lumen.

All protein expression levels were quantified from 6-12 images/tissue and expressed as MFI values of tissues stained with specific antibodies post subtraction of MFI values acquired from tissues stained with isotype control antibodies.

Analysis of blood, pulmonary vascular washout and bone marrow neutrophils by flow cytometry

Mice received an i.v injection of biotin-anti-Ly6G mAb (2μg) 90min post stimulation of cremaster muscles with locally administered IL-1β (50ng) or PBS. Mice were locally injected 30min later with histamine (200μl of 30μM solution) or PBS in combination with AF647-streptavidin (400ng). Whole blood and lung vascular washout were collected 120-240min later as previously described (14, 15), a method that recovered ~50% of the lung pulmonary vascular neutrophils. Bone marrow was isolated from 1 femur/animal. The samples were then analysed using an LSR Fortessa flow cytometer (Becton Dickinson) and FlowJo software (TreeStar). Following doublets exclusion, neutrophils from *LysM-EGFP-ki* and WT mice were gated as LysM-EGFP^{high}/GR-1^{high} or GR-1^{high}/CD115^{-}, respectively. Leukocyte numbers were determined using fluorescent counting beads.

Analysis of lung vascular leakage

Pulmonary vascular leakage was quantified by adapting published methods (26). Briefly, mice were injected i.v. with crimson-(625/645)-microbeads (20nm in diameter, 9.1x10^{13} beads;ThermoFisher), biotin-anti-Ly6G (2μg) and AF555-anti-CD31 mAb (10μg) in 150μl sterile PBS, 90min post-IL-1β-stimulation of cremaster muscles (50ng in 200μL of PBS). Thirty minutes later, mice were injected i.s. with histamine (200μl of 30μM solution) or PBS in combination with Atto425-streptavidin (400ng, Sigma-Aldrich, Poole, UK) for 120min. At the end of the reaction, mice were sacrificed, the descending vena cava was clamped and ice-cold PFA (2% in PBS) was perfused via the right ventricle. Lung lobes were excised and placed on top of a cover slip and were imaged immediately in situ with an inverted Zeiss 800 confocal laser scanning microscope. The MFI of fluorescent beads present in the extravascular space (from 5-7 images/tissue from different lung lobes) was quantified as a measure

of lung vascular leakage. For this purpose, an isosurface was generated using the anti-CD31 mAb to exclude fluorescent signal of beads inside the vascular lumen. To quantitatively analyse the association between strept$^+$ neutrophils and regions of vascular leakage, we arbitrarily defined strept$^+$ neutrophil regions as areas that expressed at least one strept$^+$ neutrophil within a perimeter of 60μm. Control areas within the same image were defined as similar size regions that were devoid of strept$^+$ neutrophils.

Statistical analysis

Data analysis was performed using GraphPad Prism 6 (GraphPad software). Results are expressed as mean±SEM and the n numbers for each dataset is provided in the figure legends. Statistical significance was assessed by 2 tailed Student's *t* test, one-way or two-way ANOVA followed by Bonferroni's post-hoc test. A P value less than 0.05 was considered significant**.**

Study approval

All in vivo experiments were conducted under the UK legislation according to the Animal Scientific Procedures Act 1986, with all procedures being conducted in accordance with UK Home Office regulations.

AUTHOR CONTRIBUTIONS

C.O-W., R.J., M-B.V. and S.N. designed the experiments; C.O-W. and R.J. did most of the experiments, compiled and analysed the data; C.O-W. initiated the experimental works. A.B and L.R. contributed to certain key experiments. C.O-W., and R.J. prepared the figures; K.A. and D.B. conducted the mathematical modelling; B.M., A.F.N., T.G., M.S., and M.G were involved in specific experiments; D.V. provided resources and advised on experimental protocols; C.O-W., R.J., M-B.V. and S.N. wrote the manuscript; M-B.V and S.N. funded the work and provided overall research supervision; S.N. conceived the project.

ACKNOWLEDGEMENTS

This work was supported by funds from the Wellcome Trust (098291/Z/12/Z to S.N.) and British Heart Foundation (PG/17/85/33395 to R.J., M-B.V. and S.N. and PG/14/62/31034 to M-B.V. and S.N.), and from the Deutsche Forschungsgemeinschaft (SFB1348, B01 to D.V.). C.O-W. is funded by a BBSRC/GSK PhD studentship, R.J. is supported by fellowships from the “Fondation pour la Recherche Medicale FRM” (award SPE20170336775), Fondation Bettencourt Schueller (Prix Jeunes Chercheurs 2017) and the People Programme (Marie Curie Actions) of the EU’s 7th Framework Programme (FP7/2007-2013) under REA grant agreement n°608765, K.A. is funded by Medical Research Council (MR/P003214/1 to K.A.). This work was supported by the CMR Advanced Bio-Imaging Facility, which has been established through generous funds from the Wellcome Trust, the British Heart Foundation, Barts Charity and QMUL. We thank Professors Tim Williams, Donald M. McDonald and Antal Rot for critical assessment.

COMPETING INTERESTS

The authors have declared that no conflict of interest exists.

REFERENCES

1. Phillipson M, Kubes P. The neutrophil in vascular inflammation. *Nat Med.* 2011;17(11):1381-90.
2. Weis SM, Cheresh DA. Pathophysiological consequences of VEGF-induced vascular permeability. *Nature.* 2005;437(7058):497-504.
3. Nourshargh S, Alon R. Leukocyte migration into inflamed tissues. *Immunity.* 2014;41(5):694-707.
4. Vestweber D. How leukocytes cross the vascular endothelium. *Nat Rev Immunol.* 2015;15(11):692-704.
5. Vestweber D, Wessel F, and Nottebaum AF. Similarities and differences in the regulation of leukocyte extravasation and vascular permeability. *Semin Immunopathol.* 2014;36(2):177-92.
6. Girbl T, et al. Distinct compartmentalization of the chemokines CXCL1 and CXCL2 and the atypical receptor ACKR1 determine discrete stages of neutrophil diapedesis. *Immunity.* 2018;49(6):1062-76 e6.
7. Bates DO. Vascular endothelial growth factors and vascular permeability. *Cardiovasc Res.* 2010;87(2):262-71.
8. Dejana E, Vestweber D. The role of VE-cadherin in vascular morphogenesis and permeability control. *Prog Mol Biol Transl Sci.* 2013;116:119-44.
9. Wessel F, et al. Leukocyte extravasation and vascular permeability are each controlled in vivo by different tyrosine residues of VE-cadherin. *Nat Immunol.* 2014;15(3):223-30.
10. Baluk P, Bolton P, Hirata A, Thurston G, and McDonald DM. Endothelial gaps and adherent leukocytes in allergen-induced early- and late-phase plasma leakage in rat airways. *Am J Pathol.* 1998;152(6):1463-76.
11. Hurley JV. An electron microscopic study of leucocytic emigration and vascular permeability in rat skin. *Aust J Exp Biol Med Sci.* 1963;41:171-86.
12. Wedmore CV, Williams TJ. Control of vascular permeability by polymorphonuclear leukocytes in inflammation. *Nature.* 1981;289(5799):646-50.
13. DiStasi MR, Ley K. Opening the flood-gates: how neutrophil-endothelial interactions regulate permeability. *Trends Immunol.* 2009;30(11):547-56.

14. Woodfin A, et al. The junctional adhesion molecule JAM-C regulates polarized transendothelial migration of neutrophils in vivo. *Nat Immunol.* 2011;12(8):761-9.

15. Colom B, et al. Leukotriene B_4-neutrophil elastase axis drives neutrophil reverse transendothelial cell migration in vivo. *Immunity.* 2015;42(6):1075-86.

16. Jones DA, Abbassi O, McIntire LV, McEver RP, and Smith CW. P-selectin mediates neutrophil rolling on histamine-stimulated endothelial cells. *Biophys J.* 1993;65(4):1560-9.

17. Kubes P, Kanwar S. Histamine induces leukocyte rolling in post-capillary venules. A P-selectin-mediated event. *J Immunol.* 1994;152(7):3570-7.

18. Shaftel SS, Carlson TJ, Olschowka JA, Kyrkanides S, Matousek SB, and O'Banion MK. Chronic interleukin-1β expression in mouse brain leads to leukocyte infiltration and neutrophil-independent blood brain barrier permeability without overt neurodegeneration. *J Neurosci.* 2007;27(35):9301-9.

19. Biondo C, et al. The interleukin-1β/CXCL1/2/neutrophil axis mediates host protection against group B streptococcal infection. *Infect Immun.* 2014;82(11):4508-17.

20. Frye M, et al. Interfering with VE-PTP stabilizes endothelial junctions in vivo via Tie-2 in the absence of VE-cadherin. *J Exp Med.* 2015;212(13):2267-87.

21. Winderlich M, et al. VE-PTP controls blood vessel development by balancing Tie-2 activity. *The J Cell Biol.* 2009;185(4):657-71.

22. Corada M, et al. Vascular endothelial-cadherin is an important determinant of microvascular integrity in vivo. *Proc Natl Acad Sci U S A.* 1999;96(17):9815-20.

23. Robertson AL, et al. A zebrafish compound screen reveals modulation of neutrophil reverse migration as an anti-inflammatory mechanism. *Sci Transl Med.* 2014;6(225):225ra29.

24. Wang J, Hossain M, Thanabalasuriar A, Gunzer M, Meininger C, and Kubes P. Visualizing the function and fate of neutrophils in sterile injury and repair. *Science.* 2017;358(6359):111-6.

25. Yoo SK, Huttenlocher A. Spatiotemporal photolabeling of neutrophil trafficking during inflammation in live zebrafish. *J Leukoc Biol.* 2011;89(5):661-7.

26. Le CT, et al. Synergistic actions of blocking angiopoietin-2 and tumor necrosis factor-α in suppressing remodeling of blood vessels and lymphatics in airway inflammation. *Am J Pathol.* 2015;185(11):2949-68.

27. Arfors KE, Lundberg C, Lindbom L, Lundberg K, Beatty PG, and Harlan JM. A monoclonal antibody to the membrane glycoprotein complex CD18 inhibits polymorphonuclear leukocyte accumulation and plasma leakage in vivo. *Blood.* 1987;69(1):338-40.

28. Gautam N, Herwald H, Hedqvist P, and Lindbom L. Signaling via β2 integrins triggers neutrophil-dependent alteration in endothelial barrier function. *J Exp Med.* 2000;191(11):1829-39.

29. Finsterbusch M, Voisin MB, Beyrau M, Williams TJ, and Nourshargh S. Neutrophils recruited by chemoattractants in vivo induce microvascular plasma protein leakage through secretion of TNF. *J Exp Med.* 2014;211(7):1307-14.

30. Kenne E, et al. Neutrophils engage the kallikrein-kinin system to open up the endothelial barrier in acute inflammation. *FASEB J.* 2019;33(2):2599-609.

31. Scapini P, et al. CXCL1/macrophage inflammatory protein-2-induced angiogenesis in vivo is mediated by neutrophil-derived vascular endothelial growth factor-A. *J Immunol.* 2004;172(8):5034-40.

32. Buckley CD, et al. Identification of a phenotypically and functionally distinct population of long-lived neutrophils in a model of reverse endothelial migration. *J Leukoc Biol.* 2006;79(2):303-11.

33. Mathias JR, Perrin BJ, Liu TX, Kanki J, Look AT, and Huttenlocher A. Resolution of inflammation by retrograde chemotaxis of neutrophils in transgenic zebrafish. *J Leukoc Biol.* 2006;80(6):1281-8.

34. Nourshargh S, Renshaw SA, and Imhof BA. Reverse migration of neutrophils: where, when, how, and why? *Trends Immunol.* 2016;37(5):273-86.

35. Tharp WG, et al. Neutrophil chemorepulsion in defined interleukin-8 gradients in vitro and in vivo. *J Leukoc Biol.* 2006;79(3):539-54.

36. Bradfield PF, et al. JAM-C regulates unidirectional monocyte transendothelial migration in inflammation. *Blood.* 2007;110(7):2545-55.

37. Thiriot A, et al. Differential DARC/ACKR1 expression distinguishes venular from non-venular endothelial cells in murine tissues. *BMC Biol.* 2017;15(1):45.

38. Graham GJ, Handel TM, and Proudfoot AEI. Leukocyte adhesion: reconceptualizing chemokine presentation by glycosaminoglycans. *Trends Immunol.* 2019;40(6):472-81.

39. Novitzky-Basso I, Rot A. Duffy antigen receptor for chemokines and its involvement in patterning and control of inflammatory chemokines. *Front Immunol.* 2012;3:266.

40. Elks PM, et al. Activation of hypoxia-inducible factor-1α (Hif-1α) delays inflammation resolution by reducing neutrophil apoptosis and reverse migration in a zebrafish inflammation model. *Blood.* 2011;118(3):712-22.

41. Harvie EA, Huttenlocher A. Neutrophils in host defense: new insights from zebrafish. *J Leukoc Biol.* 2015;98(4):523-37.

42. Nourshargh S, Marelli-Berg FM. Transmigration through venular walls: a key regulator of leukocyte phenotype and function. *Trends Immunol.* 2005;26(3):157-65.

43. Woodfin A, et al. ICAM-1-expressing neutrophils exhibit enhanced effector functions in murine models of endotoxemia. *Blood.* 2016;127(7):898-907.

44. Dangerfield J, Larbi KY, Huang MT, Dewar A, and Nourshargh S. PECAM-1 (CD31) homophilic interaction up-regulates α6β1 on transmigrated neutrophils in vivo and plays a functional role in the ability of α6 integrins to mediate leukocyte migration through the perivascular basement membrane. *J Exp Med.* 2002;196(9):1201-11.

45. Hyun YM, et al. Uropod elongation is a common final step in leukocyte extravasation through inflamed vessels. *J Exp Med.* 2012;209(7):1349-62.

46. Werr J, Xie X, Hedqvist P, Ruoslahti E, and Lindbom L. β1 integrins are critically involved in neutrophil locomotion in extravascular tissue in vivo. *J Exp Med.* 1998;187(12):2091-6.

47. Polverino E, Rosales-Mayor E, Dale GE, Dembowsky K, and Torres A. The role of neutrophil elastase inhibitors in lung diseases. *Chest.* 2017;152(2):249-62.

48. Eltzschig HK, Eckle T. Ischemia and reperfusion--from mechanism to translation. *Nat Med.* 2011;17(11):1391-401.

49. Wheeler AP, Bernard GR. Acute lung injury and the acute respiratory distress syndrome: a clinical review. *Lancet.* 2007;369(9572):1553-64.

50. Nawroth R, et al. VE-PTP and VE-cadherin ectodomains interact to facilitate regulation of phosphorylation and cell contacts. *EMBO J.* 2002;21(18):4885-95.

51. Faust N, Varas F, Kelly LM, Heck S, and Graf T. Insertion of enhanced green fluorescent protein into the lysozyme gene creates mice with green fluorescent granulocytes and macrophages. *Blood.* 2000;96(2):719-26.

FIGURES AND FIGURES LEGENDS

Figure 1. Hyperpermeability inflammatory reactions are associated with neutrophil reverse transendothelial migration. Cremaster muscles of *LysM-EGFP-ki* mice were subjected to IL-1β- or LTB_4-induced inflammation (120 and 30min, respectively), or to IR injury (40min ischemia + 1-2h reperfusion) and analysed by confocal IVM. PBS or sham-operated animals were used as control. AF647-labelled anti-CD31 mAb was injected i.s. to visualise EC junctions (red) and i.v. fluorescent (75kDa) TRITC-dextran was used to visualise vascular leakage (blue pseudocolor intensity). (**A**) Representative images of IR-stimulated cremasteric venules (see Supplemental movie 1), showing the development of an inflammatory response in terms of neutrophil migration (green GFP^{bright} neutrophils; top panels) and dextran leakage (blue; bottom panels) at the indicated times post reperfusion. Scale bars, 20μm. (**B**) Total neutrophil extravasation (n=5-12 mice/group). (**C**) Time-course of dextran accumulation in the perivascular region of a selected post-capillary venule (n=3-10 mice/group). (**D**) Representative images of an IR-stimulated cremasteric post-capillary venule at different times post reperfusion (see Supplemental movies 2 and 3) illustrating a normal neutrophil TEM (top panels) and a reverse TEM (bottom panels) event. Luminal and cross-sectional views with arrows indicating the direction of motility of the indicated neutrophil. Scale bars, 5μm. (**E**) Frequency of neutrophil reverse TEM events in relation to total TEM events of 20.7±2.1 (IL-1β), 31.3±5.9 (LTB_4) and 15±2.4 (IR injury) per 300μm venular segments within 2h microscopy periods (mean±SEM, n=6-9 mice/group). (**F**) Temporal association of dextran leakage and cumulative frequency of neutrophil reverse TEM (n=4 mice). Data are mean±SEM (each dot represents one mouse/independent experiment). Statistically significant differences from PBS (**B**) or IL-1β (**E**)-treated mice are indicated by **p<0.01,***p<0.001, one-way ANOVA followed by Bonferroni's post-hoc test.

Figure 2. Induction of microvascular leakage promotes neutrophil reverse transendothelial migration. Cremaster muscles of *LysM-EGFP-ki* mice were subjected to IL-1β-induced inflammation for 120min and analysed by confocal IVM. AF647-labelled anti-CD31 mAb (i.s.) and 75kDa-TRITC-dextran (i.v.) were used to visualise EC junctions (red) and vascular leakage (blue pseudocolor intensity), respectively. Mice were superfused with histamine (30μM) or injected i.v. with VEGF (4μg) 2h post-IL-1β stimulation. (**A**) Total neutrophil extravasation (n=4-5 mice/group). (**B**) Representative images of a post-capillary venular segment subjected to IL-1β+histamine stimulation at different time-points post application of histamine, illustrating neutrophil TEM and dextran leakage responses (see Supplemental movie 4). Scale bars, 20μm. (**C**) Time-course of dextran accumulation in the perivascular region of a selected post-capillary venule (n=3-9 mice/group). (**D**) Frequency of neutrophil reverse TEM events in relation to total TEM events of 15.2±2.4 (IL-1β), 19.8±2.9 (IL-

1β+Hist) and 21±3.6 (IL-1β+VEGF) per 300μm venular segments within 2h microscopy periods (mean ± SEM, n=4-10 mice/group). (**E**) Temporal association of dextran leakage and cumulative frequency of neutrophil reverse TEM (n=7-9 mice/group). Data are represented as mean±SEM (each dot represents one mouse/independent experiment). Statistically significant differences from PBS (**A**) or IL-1β (**D**)-treated mice are indicated by *p<0.05,**p<0.01,***p<0.001, one-way ANOVA followed by Bonferroni's post-hoc test.

Figure 3. Chimeric VEC-Y658F mice exhibit reduced microvascular leakage induction and neutrophil reverse TEM. (**A**) Generation of chimeric mice exhibiting *LysM-EGFP-ki* haematopoietic cells within *VEC-WT* or *VEC-Y658F* recipients. (**B**) Representative confocal IVM images of post-capillary venular segments (stained with anti-CD31; red) subjected to IL-1β+histamine stimulation at two time-points post application of histamine in chimeric *VEC-WT* and *VEC-Y658F* mice, illustrating dextran leakage (blue pseudocolor intensity). Scale bars, 10μm. (**C**) Time-course of dextran accumulation in the perivascular region of selected IL-1β-stimulated post-capillary venules in *VEC-WT* and *VEC-Y658F* chimeric mice post topical application of histamine (n=6-12 mice per group). (**D**) Total neutrophil extravasation (n=5-11 mice per group). (**E**) Frequency of neutrophil reverse TEM events in relation to total TEM events of 16.6±2.1 (*VEC-WT*) and 19.2±3.1 (*VEC-Y685F*) per 300μm venular segments within 2h microscopy periods (mean ± SEM, n=5-11 mice). Data are represented as mean±SEM (each dot represents one mouse/independent experiment). Indicated statistical differences are shown by *p<0.05, two-tailed Student's t-test (ns = not significant).

Figure 4. Stimulated microvascular leakage induces movement of small molecular weight proteins into the vascular lumen. (**A**-**D**) Cremaster muscles of WT mice were stimulated with IL-1β or TNF for 2h followed by local injection of histamine or i.v. VEGF (or corresponding vehicle), for 30min prior to collection of tissue and plasma samples for quantification of CXCL1 levels by ELISA. Mice subjected to PBS, histamine or VEGF alone were used as control (n=4-7 mice/group). (**E**) Representative images of selected IL1β-stimulated post-capillary venules showing movement of i.v. 75kDa-TRITC-dextran (marker of vascular leakage; red) and topically applied 10kDa-AF488-dextran (superfused for 10min; green) post topical superfusion of PBS vehicle (top panels) or histamine (30μM, lower panels, see Supplemental movie 5). Dashed lines indicate blood vessel borders, scale bars, 20μm. (**F** and **G**) Time-course of 75kDa-TRITC- and 10kDa-AF488-dextran accumulation in the perivascular region of selected IL-1β-stimulated post-capillary venules post superfusion of vehicle (**F**, n=3 mice) or histamine (**G**, n=3 mice). (**H**) Quantification of 10kDa-AF488-dextran in plasma samples of mice treated as detailed above (n=3 mice/group). (**I**) Schematic diagram illustrating the

mathematical calculation of the Péclet number (*Pe*) (see Supplemental Figure 4). Data are represented as mean±SEM (each dot represents one mouse/independent experiment). Statistically significant differences from PBS (**A**-**D**) or IL1β+vehicle (**H**) are indicated by *p<0.05,**p<0.01,***p<0.001, between groups as indicated by lines by #p<0.05, one-way ANOVA followed by Bonferroni's post-hoc test or two-tailed Student's t-test (ns = not significant).

Figure 5. Vascular leakage induction promotes trafficking of tissue chemokine through venular walls. Cremaster muscles were injected locally with IL-1β (50ng) and human CXCL8 (hCXCL8, 500ng) for 1h, followed by i.s. injection of vehicle (control) or histamine for a further 1h. (**A**) Representative confocal images of post-capillary venules stained for hCXCL8 within an EC (labelled by anti-CD31) isosurface mask with an enlarged image of the boxed region. Scale bars, 2μm. (**B**) Quantification of hCXCL8 MFI on EC body and junctions (n=8 mice/group). (**C**-**F**) Plasma levels of locally applied hCXCL8 in WT mice (**C**), *VEC-WT* and *VEC-Y685F* mice (**D**), in mice treated with a control or anti-VE-PTP Ab (200μg, i.v.) (**E**), or treated with an anti-VE-cadherin mAb (i.s. BV13, 100μg), or a control mAb (non-blocking anti-CD31 mAb, 100μg) for 3h prior to local administration of tissues with hCXCL8 for 1h (n=4-8 mice/group) (**F**). Data are represented as mean±SEM (each dot represents one mouse/independent experiment). Statistically significant differences cell body vehicle vs cell body histamine and Jn vehicle vs Jn histamine groups were analysed by one-way ANOVA followed by Bonferroni's post-hoc test (*p<0.05,**p<0.01). Differences between the other indicated groups are shown by *p<0.05,**p<0.01,***p<0.001 analysed by two-way ANOVA followed by Bonferroni's post-hoc test or two-tailed paired or unpaired Student's t-test.

Figure 6. Systemic CXCL1 promotes neutrophil reverse TEM. Cremaster muscles of *LysM-EGFP-ki* mice were stimulated with IL-1β (50ng for 2h) followed by topical superfusion of histamine onto exteriorised tissues or subjected to IR injury. Blocking anti-CXCL1 mAb (1mg/kg), or control IgG, was injected i.v. 30min before exteriorisation of tissues or at the point of tissue reperfusion. (**A**) Time-course of dextran accumulation in the perivascular region of selected stimulated post-capillary venules. Tissue dextran accumulation is represented as normalised MFI (n=4-6 mice per group). (**B**) Total neutrophil extravasation (n=4-5 mice/group) and (**C**) frequency of neutrophil reverse TEM events in relation to total TEM events of 14±2 (control mAb) and 20±2.9 (anti-CXCL1 mAb) per 300μm venular segments within 2h microscopy periods (mean ± SEM, (n=5-6 mice/group). (**D**) Total neutrophil extravasation (n=3-6 mice/group) and (**E**) frequency of neutrophil reverse TEM events in relation to total TEM events of 26.7±3.8 (control mAb) and 26±4.3 (anti-CXCL1) per 300μm venular segments within 2h microscopy periods (mean ± SEM, n=3-7 mice/group). (**F**) Cremaster muscles of

LysM-EGFP-ki mice were stimulated with IL-1β (50ng for 2h) followed by i.v. injection of murine rCXCL1 (50ng). Frequency of neutrophil reverse TEM events in relation to total TEM events of 16±2.8 (IL-1β) and 12.9±1.8 (IL-1β+CXCL1) per 300μm venular segments within 2h microscopy periods (mean±SEM, n=5-7 mice/group). Data are represented as mean±SEM (each dot represents one mouse/independent experiment). Statistically significant differences from control mAb-treated groups (**C** and **E**) or IL-1β treated-tissues (**F**) are shown by *p<0.05,***p<0.001, two-tailed Student's t-test.

Figure 7. Development of an in vivo labelling strategy for tracking rTEM neutrophils. (**A**) Diagram detailing the labelling method. Cremaster muscles of *LysM-EGFP-ki* mice were stimulated with IL-1β (50ng for 2h) followed by an i.v. injection of biotinylated-anti-Ly6G (2μg) to label blood neutrophils at t=90min. The tissues were superfused with histamine (30μM) or vehicle in conjunction with AF647-streptavidin (1μg/ml) for 2h. (**B**) Representative confocal image of an IL-1β–stimulated post-capillary venule illustrating the extent of AF647-Strept labelling of neutrophils at different stages of trafficking (left panel). Right panels shown enlarged images of the boxed regions and illustrate examples of AF647-Strept$^-$ luminal, AF647-Strept$^+$ sub-EC and AF647-Strept$^+$ interstitial neutrophils. Scale bars, 5μm. (**C**) Representative confocal IVM images of a tissue stimulated with IL-1β+Hist (see Supplemental movie 6) illustrating the effective labelling of an rTEM event. The exemplified neutrophil shows that once the cell has breached an EC junction, the leading body part in the sub-EC space rapidly becomes AF647-Strept$^+$ whilst the luminal body segment remains AF647-Strept$^-$. The AF647-Strept$^+$ neutrophil can be easily tracked as it migrates in a reverse manner towards the vascular lumen and re-enters the blood stream. Luminal and cross-sectional views are shown with the arrows indicating the direction of motility of the indicated neutrophil. Scale bars, 3μm. (**D**) Fluorescence intensity of AF647-streptavidin on neutrophils in the venular lumen, tissue and cells exhibiting rTEM (n=4 mice/group) during an IL-1β+histamine reaction. Data are represented as mean±SEM (each dot represents one mouse/independent experiment). Statistically significant differences from luminal neutrophils is shown by **p<0.01,***p<0.001, one-way ANOVA followed by Bonferroni's post-hoc test.

Figure 8. Labelled rTEM neutrophils are present in blood and pulmonary vasculature and show an activated phenotype. (**A** and **B**) *LysM-EGFP-ki* mice were subjected to local cremaster muscle stimulation with IL-1β (2h) and an i.v. injection of biotinylated-anti-Ly6G (2μg) at t=90min. The tissues were then superfused with histamine (30μM) or vehicle in conjunction with AF647-streptavidin (1μg/ml) for 2h. Peripheral blood was analysed for the frequency of AF647-Strept$^+$ neutrophils. (**A**) Representative flow cytometry profiles and (**B**) frequency of AF647-Strept$^+$ neutrophils (LysM-

GFP^{high}/Gr-1^{high}) (n=6 mice/group). (**C**-**G**) WT mice were subjected to cremaster muscle stimulation with IL-1β or PBS for 2h followed by i.v. injection of biotinylated-anti-Ly6G (2μg) at t=90min. The mice then received an i.s. injection of AF647-Strept (400ng) co-administered with histamine (200μl of 30μM solution) or PBS for 2h. Peripheral blood and pulmonary vascular washout samples were analysed by FACS. (**C**) Expression of indicated markers on AF647-Strept^{+} neutrophils relative to levels on AF647-Strept^{-} neutrophils in blood samples collected from mice subjected to IL-1β+histamine, as measured by Geometric MFI (gMFI) (n=5-8 mice/group). (**D**) Representative flow cytometry profiles and (**E**) frequency of pulmonary vascular washout AF647-Strept^{+} neutrophils (Gr-1^{high}/CD115^{-}) (n=4-8 mice/group). (**F**) Representative FACS histograms and (**G**) expression of indicated markers on AF647-Strept^{+} neutrophils relative to levels on AF647-Strept^{-} neutrophils in pulmonary vascular washout samples collected from mice stimulated with IL-1β+histamine, as measured by gMFI (n=6-9 mice/group). Data are represented as mean±SEM (each dot represents one mouse/independent experiment). Statistically significant differences from IL-1β (**B**), gMFI of indicated markers of blood AF647-Strept^{-} neutrophils (**C**), PBS (**E**) and gMFI of indicated markers on pulmonary vascular washout AF647-Strept^{-} neutrophils (**G**) are shown by *p<0.05,***p<0.01 or by indicated comparisons ##p<0.01, two-tailed Student's t-test or one-way ANOVA followed by Bonferroni's post-hoc test (ns=not significant).

Figure 9. Accumulation of labelled rTEM neutrophils in lungs is linked with lung injury. The cremaster muscles of *LysM-EGFP-ki* mice were locally stimulated with IL-1β or PBS (2h). Mice were injected i.v. with AF555-anti-CD31 mAb (10μg), biotin-anti-Ly6G mAb and fluorescent microspheres (20nm diameter, 9.1x10^{13} beads) at t=90min to label the vasculature, neutrophils and to quantify vascular leakage, respectively. To induce and to track rTEM neutrophils stemming from the cremaster muscles, tissues were additionally stimulated with locally applied histamine or vehicle (PBS) in combination with Atto425-Streptavidin (AT425-Strept, 400ng) for 120min. The lungs were then analysed by confocal microscopy. (**A**) Representative confocal images of alveolar capillaries in whole-mount imaged lungs of mice in which the cremaster muscles were locally stimulated as indicated (CD31-labelled vessels, red; neutrophils, blue; extravascular beads, green). Scale bars, 20μm. (**B**) Lung vascular leakage as quantified by accumulation (MFI) of extravascular beads (n=4-6 mice/group) and (**C**) number of AT425-Strept^{+} neutrophils per field of view (n=4-6 mice per group), in mice subjected to indicated cremaster muscle stimulations. (**D**) Correlation of the number of AT425-Strept^{+} neutrophils and extravascular beads in lung tissues (n=4-6 mice/group). Line indicated linear regression and dashed lines 95% confidence band (Spearman r=0.7). (**E**) High magnification images of lung sections showing AT425-Strept^{+} neutrophils in close apposition to sites of extravascular

fluorescent bead accumulation. Scale bars, 3μm. (**F**) Lung vascular leakage in close proximity (<60μm) of AT425-Strept$^-$ neutrophils or AT425-Strept$^+$ neutrophils (n=6 mice/group). Data are represented as mean±SEM (each dot represents one mouse/independent experiment). Statistically significant differences from PBS or indicated group are shown by **p<0.01,***p<0.001, and between indicated groups by ##p<0.01,###p<0.01, one-way ANOVA followed by Bonferroni's post-hoc test or paired t-test or Spearman's rank correlation test (ns=not significant).

Figure 10. Schematic diagram of the cascade of events that link a local hyperpermeability inflammatory reaction to neutrophil rTEM and development of lung injury.

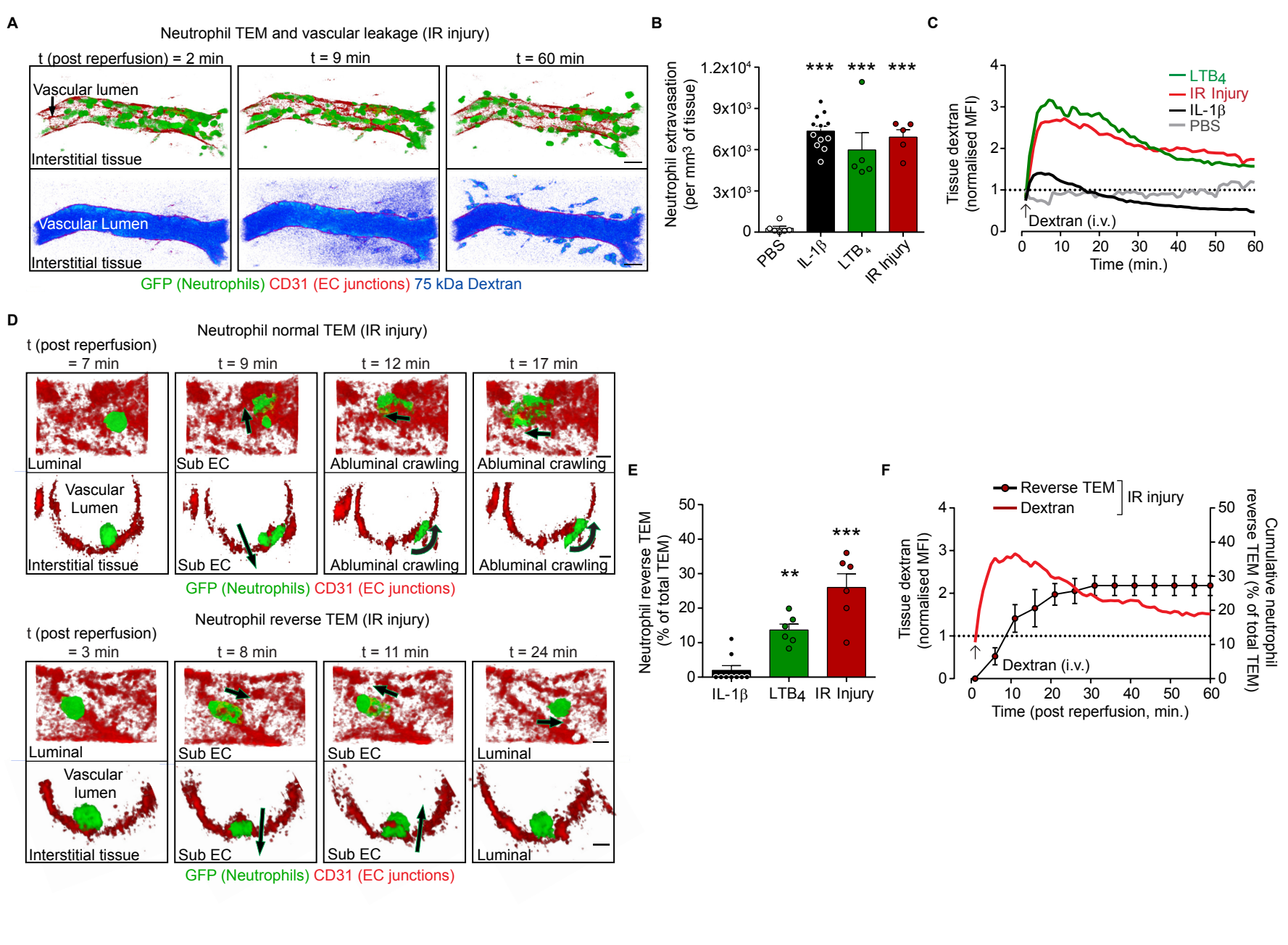
A
Neutrophil TEM and vascular leakage (IR injury)
t (post reperfusion) = 2 min
t = 9 min
t = 60 min
Vascular lumen
Interstitial tissue
Vascular Lumen
Interstitial tissue
GFP (Neutrophils) CD31 (EC junctions) 75 kDa Dextran
B
Neutrophil extravasation (per mm3 of tissue)
1.2x10^4
9x10^3
6x10^3
3x10^3
0
***
***
***
PBS
IL-1β
LTB4
IR Injury
C
Tissue dextran (normalised MFI)
LTB4
IR Injury
IL-1β
PBS
Dextran (i.v.)
Time (min.)
D
Neutrophil normal TEM (IR injury)
t (post reperfusion) = 7 min
t = 9 min
t = 12 min
t = 17 min
Luminal
Sub EC
Abluminal crawling
Abluminal crawling
Vascular Lumen
Interstitial tissue
Sub EC
Abluminal crawling
Abluminal crawling
GFP (Neutrophils) CD31 (EC junctions)
Neutrophil reverse TEM (IR injury)
t (post reperfusion) = 3 min
t = 8 min
t = 11 min
t = 24 min
Luminal
Sub EC
Sub EC
Luminal
Vascular lumen
Interstitial tissue
Sub EC
Sub EC
Luminal
GFP (Neutrophils) CD31 (EC junctions)
E
Neutrophil reverse TEM (% of total TEM)
**
***
IL-1β
LTB4
IR Injury
F
Reverse TEM
Dextran
IR injury
Tissue dextran (normalised MFI)
Cumulative neutrophil reverse TEM (% of total TEM)
Dextran (i.v.)
Time (post reperfusion, min.)

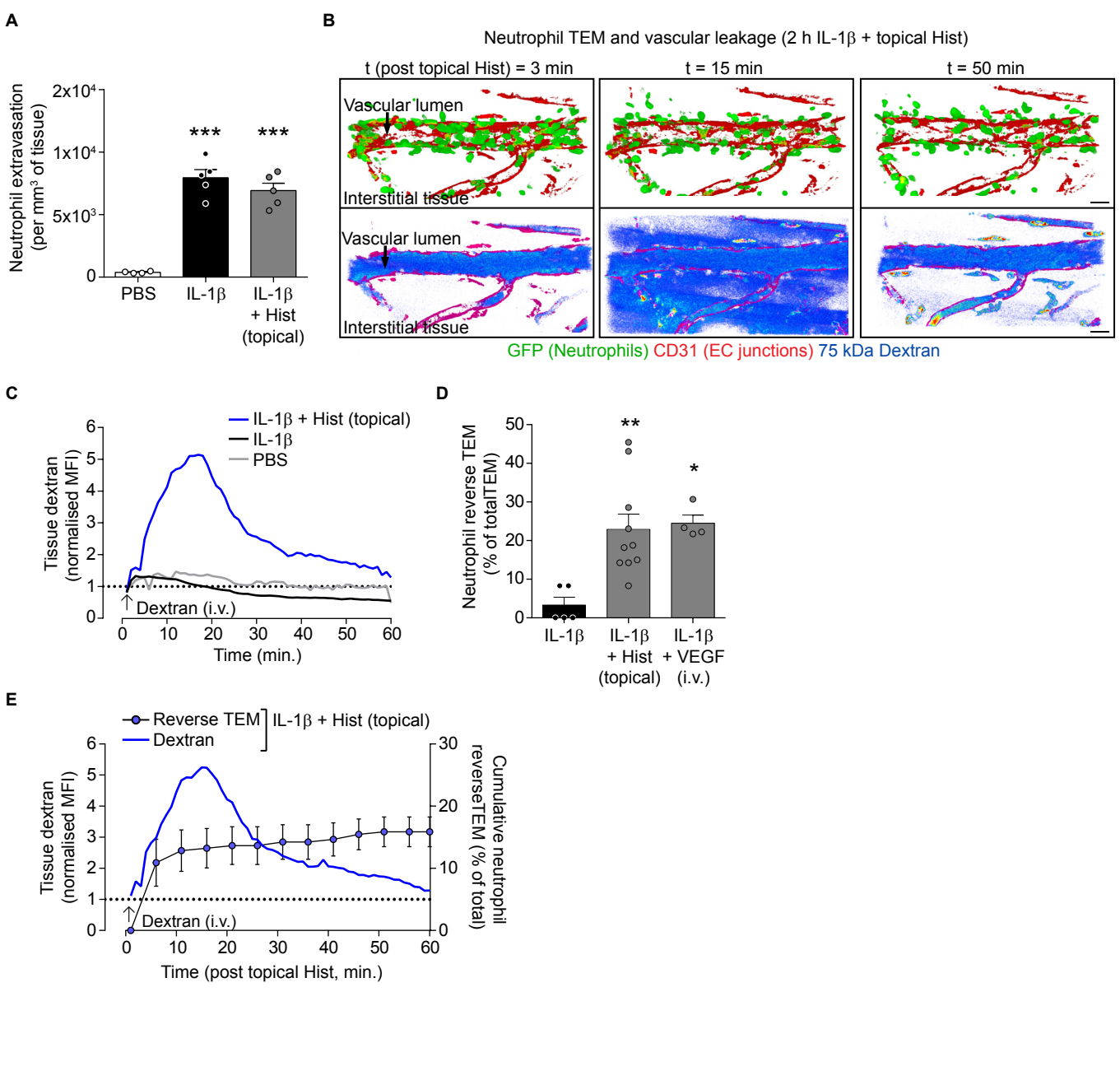
A
Neutrophil extravasation (per mm3 of tissue)
2x10^4
1x10^4
5x10^3
0
***
***
PBS
IL-1β
IL-1β + Hist (topical)
B
Neutrophil TEM and vascular leakage (2 h IL-1β + topical Hist)
t (post topical Hist) = 3 min
t = 15 min
t = 50 min
Vascular lumen
Interstitial tissue
Vascular lumen
Interstitial tissue
GFP (Neutrophils) CD31 (EC junctions) 75 kDa Dextran
C
IL-1β + Hist (topical)
IL-1β
PBS
Tissue dextran (normalised MFI)
Dextran (i.v.)
Time (min.)
D
Neutrophil reverse TEM (% of totalTEM)
**
*
IL-1β
IL-1β + Hist (topical)
IL-1β + VEGF (i.v.)
E
Reverse TEM
Dextran
IL-1β + Hist (topical)
Tissue dextran (normalised MFI)
Cumulative neutrophil reverseTEM (% of total)
Dextran (i.v.)
Time (post topical Hist, min.)

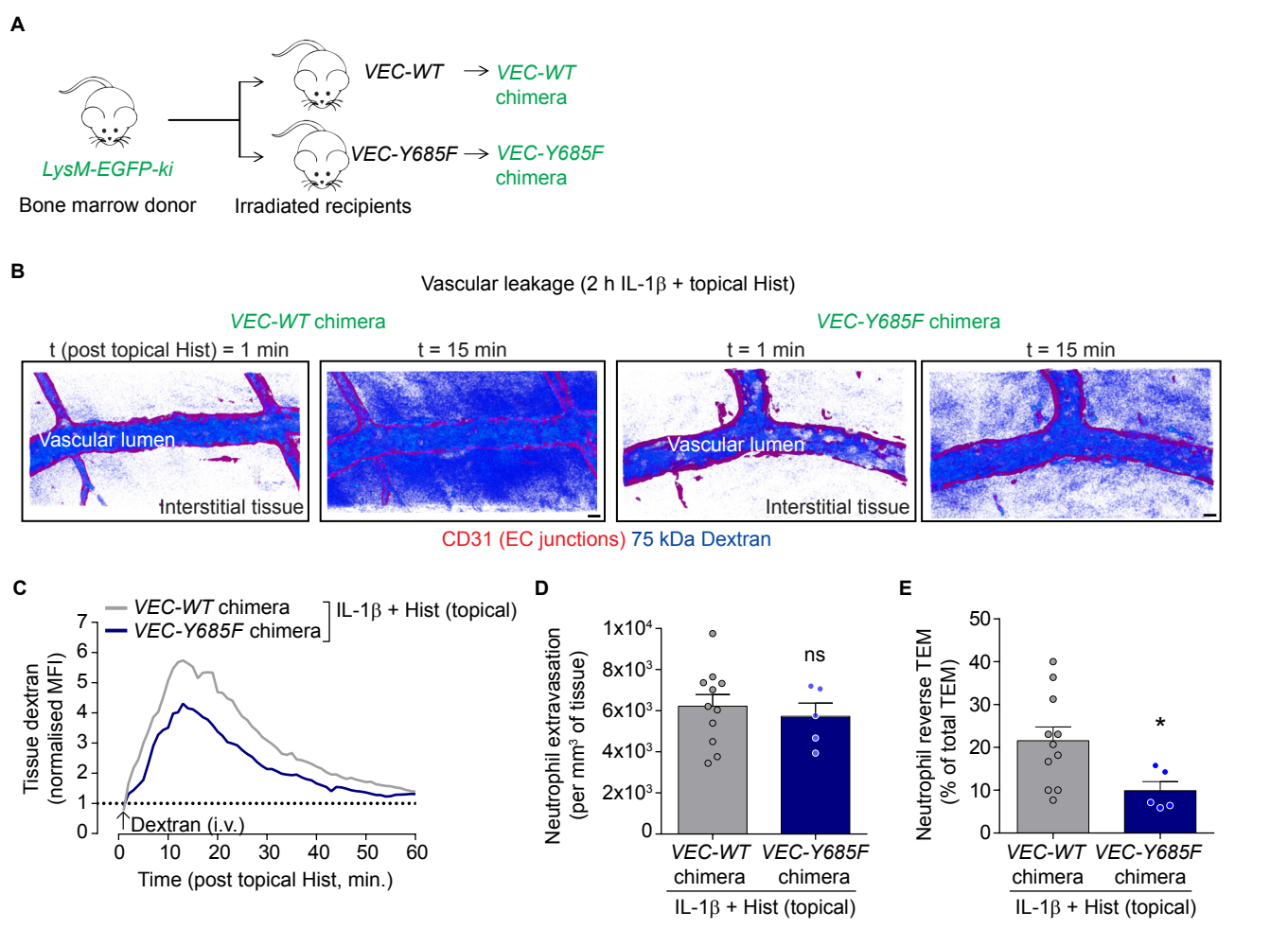
A
LysM-EGFP-ki
Bone marrow donor
VEC-WT → VEC-WT chimera
VEC-Y685F → VEC-Y685F chimera
Irradiated recipients
B
Vascular leakage (2 h IL-1β + topical Hist)
VEC-WT chimera
VEC-Y685F chimera
t (post topical Hist) = 1 min
t = 15 min
t = 1 min
t = 15 min
Vascular lumen
Interstitial tissue
Vascular lumen
Interstitial tissue
CD31 (EC junctions) 75 kDa Dextran
C
VEC-WT chimera
VEC-Y685F chimera
IL-1β + Hist (topical)
Tissue dextran (normalised MFI)
Dextran (i.v.)
Time (post topical Hist, min.)
D
Neutrophil extravasation (per mm3 of tissue)
ns
VEC-WT chimera
VEC-Y685F chimera
IL-1β + Hist (topical)
E
Neutrophil reverse TEM (% of total TEM)
*
VEC-WT chimera
VEC-Y685F chimera
IL-1β + Hist (topical)

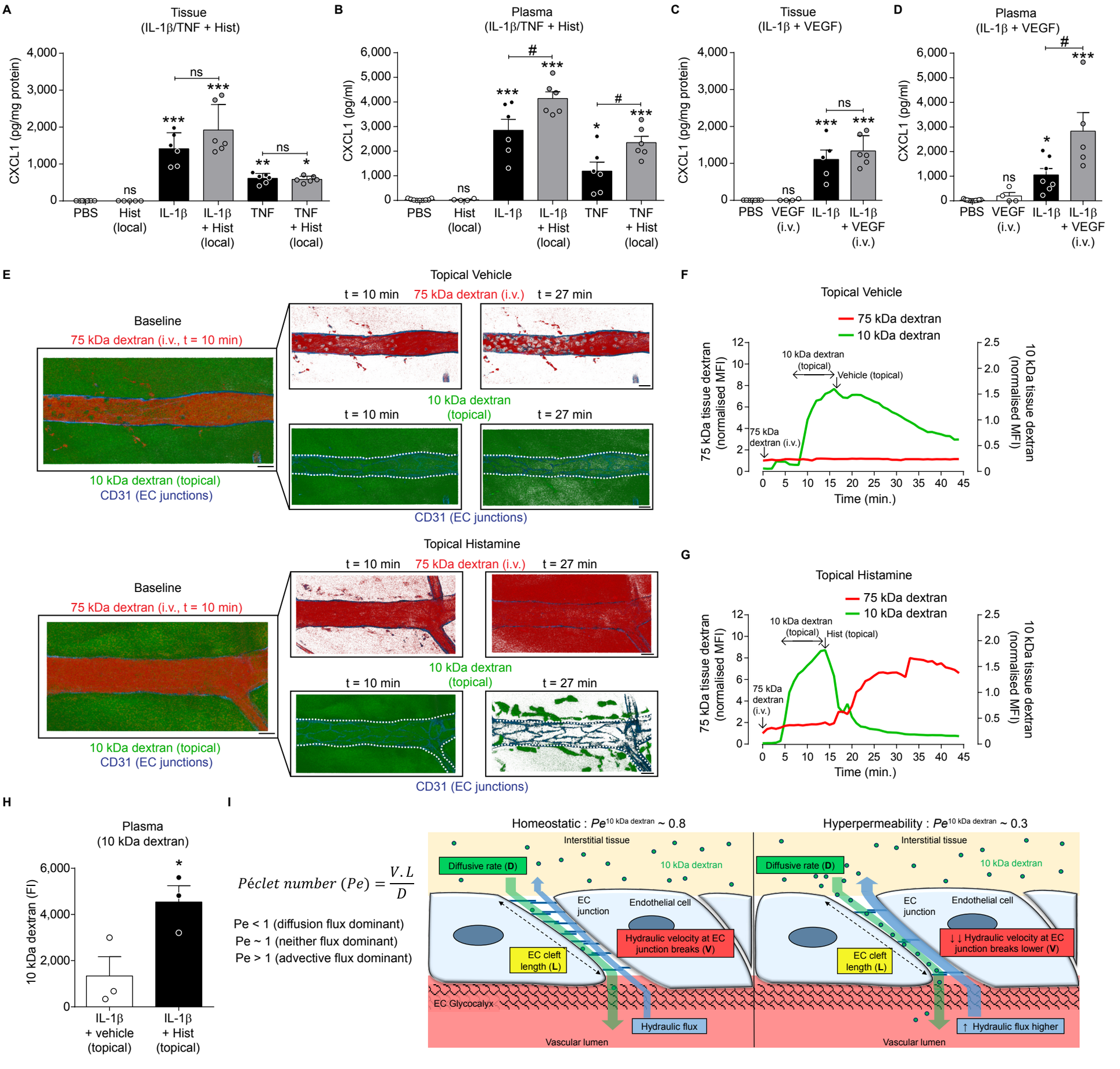

$$Péclet\ number\ (Pe) = \frac{V.L}{D}$$

Pe < 1 (diffusion flux dominant)
Pe ~ 1 (neither flux dominant)
Pe > 1 (advective flux dominant)

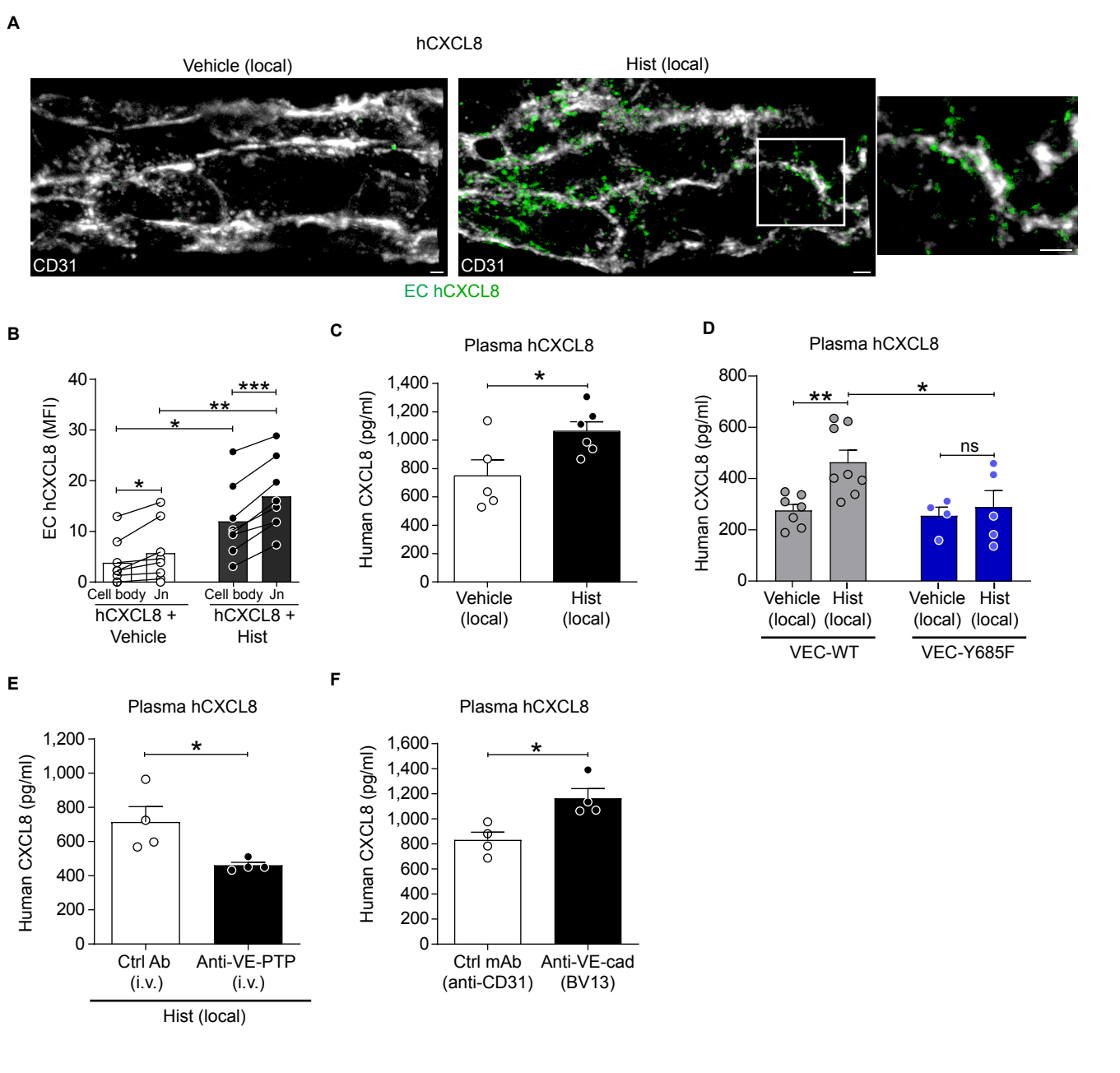
A
hCXCL8
Vehicle (local)
Hist (local)
CD31
CD31
EC hCXCL8
B
EC hCXCL8 (MFI)
40
30
20
10
0
*
*
**
***
Cell body
Jn
Cell body
Jn
hCXCL8 +
Vehicle
hCXCL8 +
Hist
C
Plasma hCXCL8
Human CXCL8 (pg/ml)
1,400
1,200
1,000
800
600
400
200
0
*
Vehicle
(local)
Hist
(local)
D
Plasma hCXCL8
Human CXCL8 (pg/ml)
800
600
400
200
0
**
*
ns
Vehicle
(local)
Hist
(local)
Vehicle
(local)
Hist
(local)
VEC-WT
VEC-Y685F
E
Plasma hCXCL8
Human CXCL8 (pg/ml)
1,200
1,000
800
600
400
200
0
*
Ctrl Ab
(i.v.)
Anti-VE-PTP
(i.v.)
Hist (local)
F
Plasma hCXCL8
Human CXCL8 (pg/ml)
1,600
1,400
1,200
1,000
800
600
400
200
0
*
Ctrl mAb
(anti-CD31)
Anti-VE-cad
(BV13)

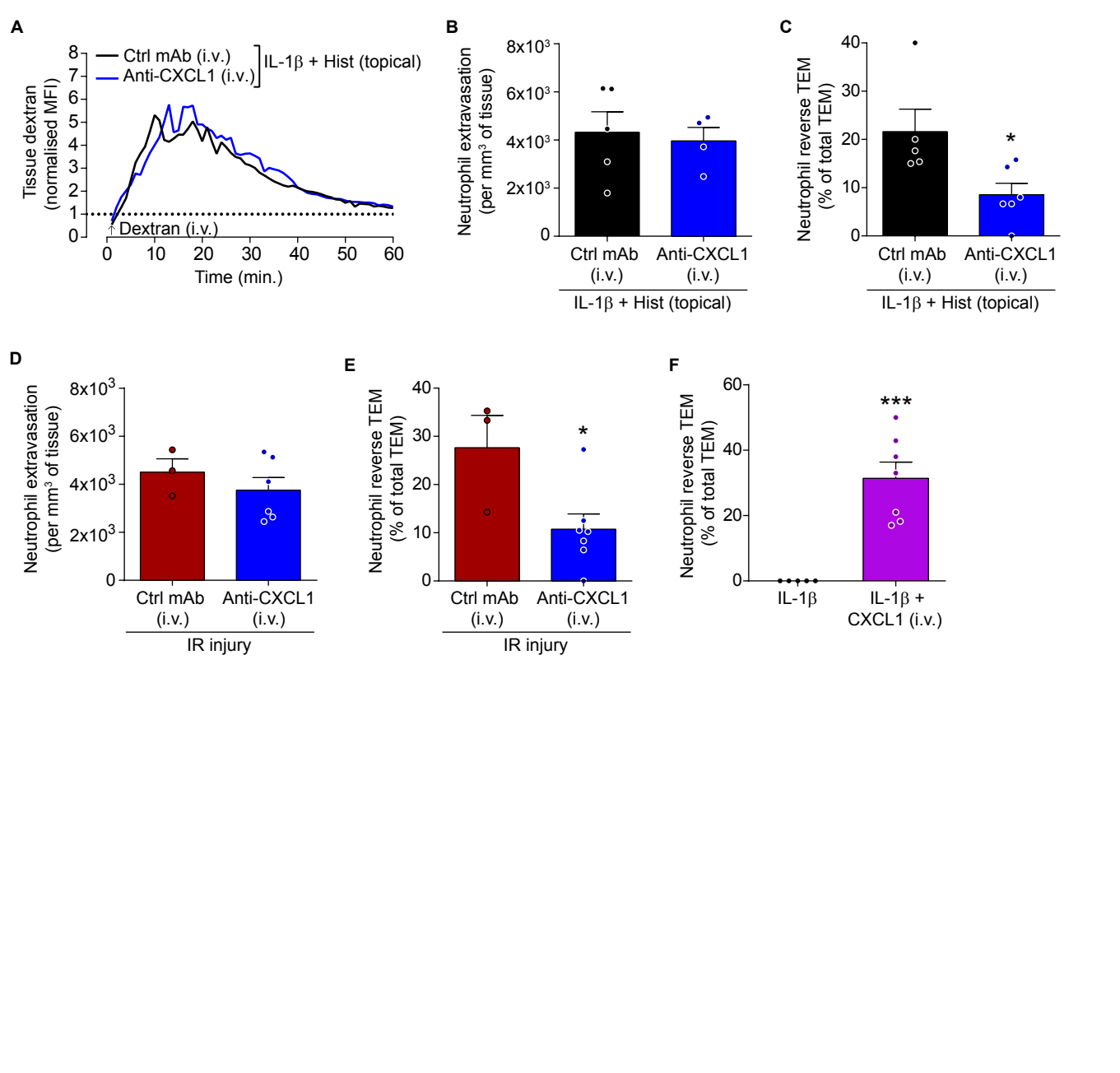
A
Ctrl mAb (i.v.)
Anti-CXCL1 (i.v.)
IL-1β + Hist (topical)
Tissue dextran (normalised MFI)
Dextran (i.v.)
Time (min.)
B
Neutrophil extravasation (per mm3 of tissue)
Ctrl mAb (i.v.)
Anti-CXCL1 (i.v.)
IL-1β + Hist (topical)
C
Neutrophil reverse TEM (% of total TEM)
Ctrl mAb (i.v.)
Anti-CXCL1 (i.v.)
IL-1β + Hist (topical)
D
Neutrophil extravasation (per mm3 of tissue)
Ctrl mAb (i.v.)
Anti-CXCL1 (i.v.)
IR injury
E
Neutrophil reverse TEM (% of total TEM)
Ctrl mAb (i.v.)
Anti-CXCL1 (i.v.)
IR injury
F
Neutrophil reverse TEM (% of total TEM)
IL-1β
IL-1β + CXCL1 (i.v.)

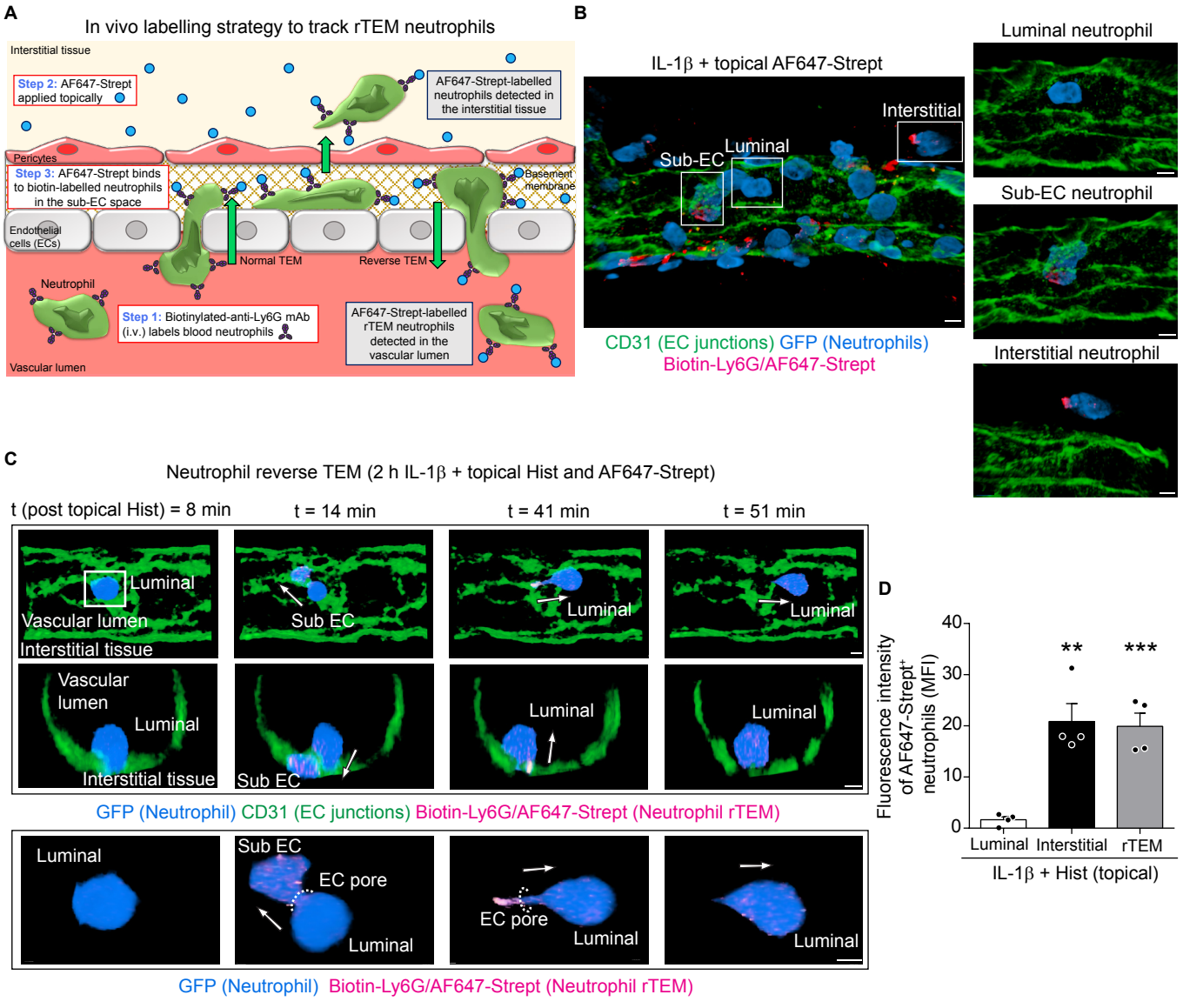
A
In vivo labelling strategy to track rTEM neutrophils
Interstitial tissue
Step 2: AF647-Strept applied topically
AF647-Strept-labelled neutrophils detected in the interstitial tissue
Pericytes
Step 3: AF647-Strept binds to biotin-labelled neutrophils in the sub-EC space
Basement membrane
Endothelial cells (ECs)
Normal TEM
Reverse TEM
Neutrophil
Step 1: Biotinylated-anti-Ly6G mAb (i.v.) labels blood neutrophils
AF647-Strept-labelled rTEM neutrophils detected in the vascular lumen
Vascular lumen
B
IL-1β + topical AF647-Strept
Interstitial
Luminal
Sub-EC
CD31 (EC junctions) GFP (Neutrophils)
Biotin-Ly6G/AF647-Strept
Luminal neutrophil
Sub-EC neutrophil
Interstitial neutrophil
C
Neutrophil reverse TEM (2 h IL-1β + topical Hist and AF647-Strept)
t (post topical Hist) = 8 min
t = 14 min
t = 41 min
t = 51 min
Luminal
Vascular lumen
Interstitial tissue
Sub EC
Vascular lumen
GFP (Neutrophil) CD31 (EC junctions) Biotin-Ly6G/AF647-Strept (Neutrophil rTEM)
EC pore
GFP (Neutrophil) Biotin-Ly6G/AF647-Strept (Neutrophil rTEM)
D
Fluorescence intensity of AF647-Strept+ neutrophils (MFI)
40
30
20
10
0
**
***
Luminal
Interstitial
rTEM
IL-1β + Hist (topical)

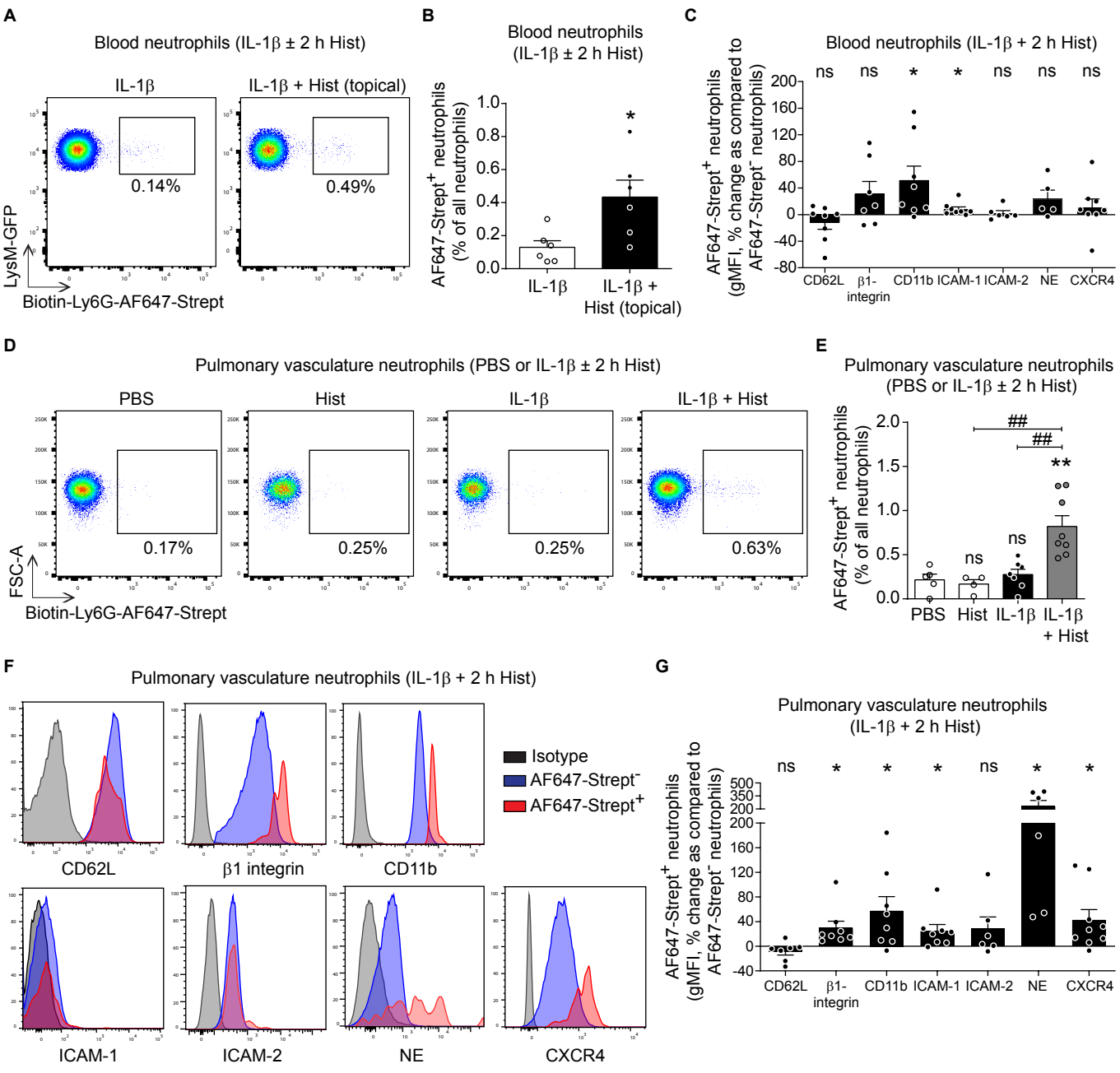
A
Blood neutrophils (IL-1β ± 2 h Hist)
IL-1β
IL-1β + Hist (topical)
0.14%
0.49%
LysM-GFP
Biotin-Ly6G-AF647-Strept
B
Blood neutrophils
(IL-1β ± 2 h Hist)
AF647-Strept+ neutrophils
(% of all neutrophils)
IL-1β
IL-1β +
Hist (topical)
C
Blood neutrophils (IL-1β + 2 h Hist)
AF647-Strept+ neutrophils
(gMFI, % change as compared to
AF647-Strept- neutrophils)
ns ns * * ns ns ns
CD62L
β1-
integrin
CD11b
ICAM-1
ICAM-2
NE
CXCR4
D
Pulmonary vasculature neutrophils (PBS or IL-1β ± 2 h Hist)
PBS
Hist
IL-1β
IL-1β + Hist
0.17%
0.25%
0.25%
0.63%
FSC-A
Biotin-Ly6G-AF647-Strept
E
Pulmonary vasculature neutrophils
(PBS or IL-1β ± 2 h Hist)
AF647-Strept+ neutrophils
(% of all neutrophils)
**
ns ns
PBS
Hist
IL-1β
IL-1β
+ Hist
F
Pulmonary vasculature neutrophils (IL-1β + 2 h Hist)
Isotype
AF647-Strept-
AF647-Strept+
CD62L
β1 integrin
CD11b
ICAM-1
ICAM-2
NE
CXCR4
G
Pulmonary vasculature neutrophils
(IL-1β + 2 h Hist)
AF647-Strept+ neutrophils
(gMFI, % change as compared to
AF647-Strept- neutrophils)
ns * * * ns * *
CD62L
β1-
integrin
CD11b
ICAM-1
ICAM-2
NE
CXCR4

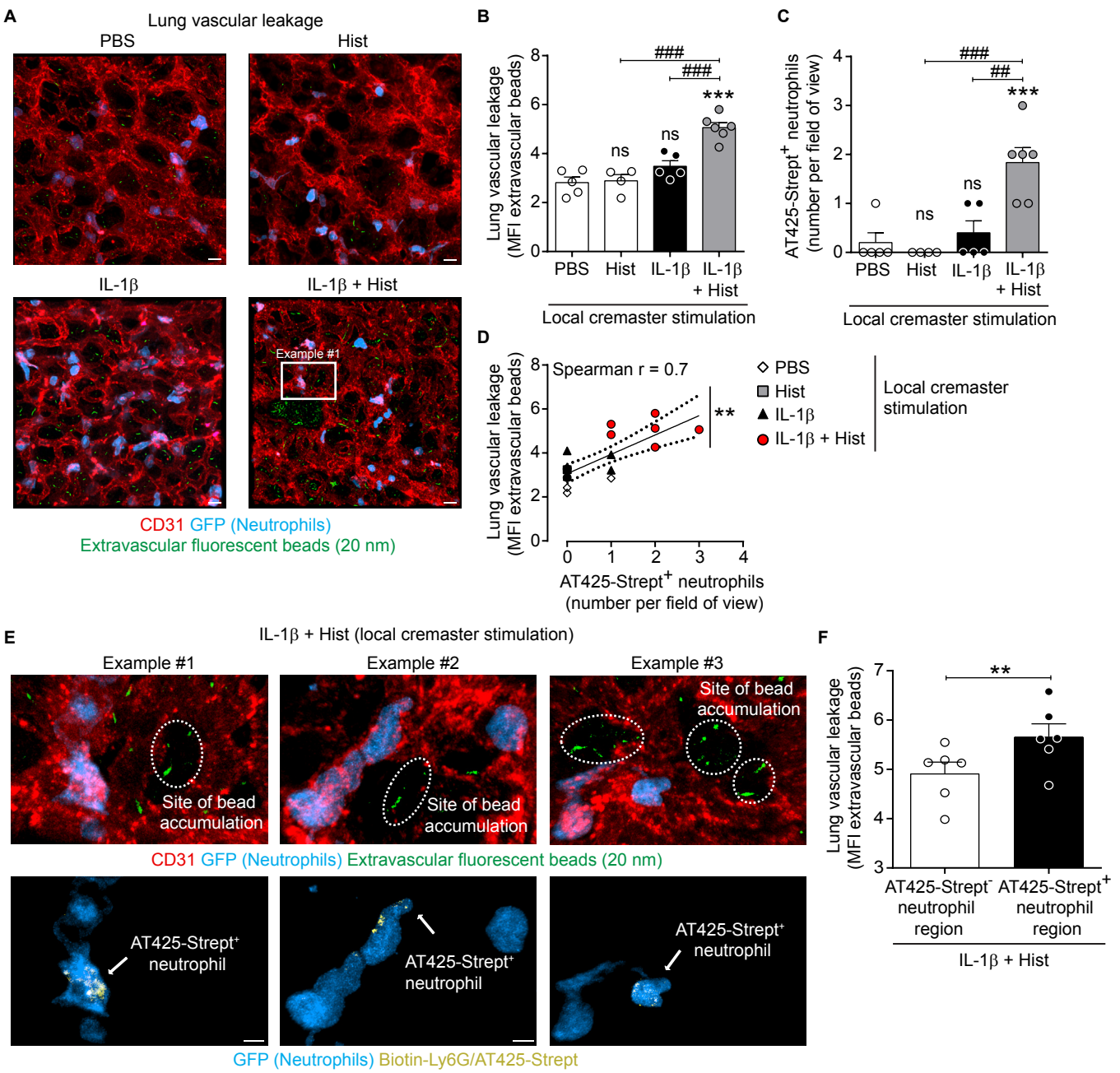
A
Lung vascular leakage
PBS
Hist
IL-1β
IL-1β + Hist
Example #1
CD31 GFP (Neutrophils)
Extravascular fluorescent beads (20 nm)
B
Lung vascular leakage (MFI extravascular beads)
###
###
***
ns
ns
PBS
Hist
IL-1β
IL-1β + Hist
Local cremaster stimulation
C
AT425-Strept+ neutrophils (number per field of view)
###
##
***
ns
ns
PBS
Hist
IL-1β
IL-1β + Hist
Local cremaster stimulation
D
Lung vascular leakage (MFI extravascular beads)
Spearman r = 0.7
**
PBS
Hist
IL-1β
IL-1β + Hist
Local cremaster stimulation
AT425-Strept+ neutrophils (number per field of view)
E
IL-1β + Hist (local cremaster stimulation)
Example #1
Example #2
Example #3
Site of bead accumulation
Site of bead accumulation
Site of bead accumulation
CD31 GFP (Neutrophils) Extravascular fluorescent beads (20 nm)
AT425-Strept+ neutrophil
AT425-Strept+ neutrophil
AT425-Strept+ neutrophil
GFP (Neutrophils) Biotin-Ly6G/AT425-Strept
F
Lung vascular leakage (MFI extravascular beads)
**
AT425-Strept- neutrophil region
AT425-Strept+ neutrophil region
IL-1β + Hist

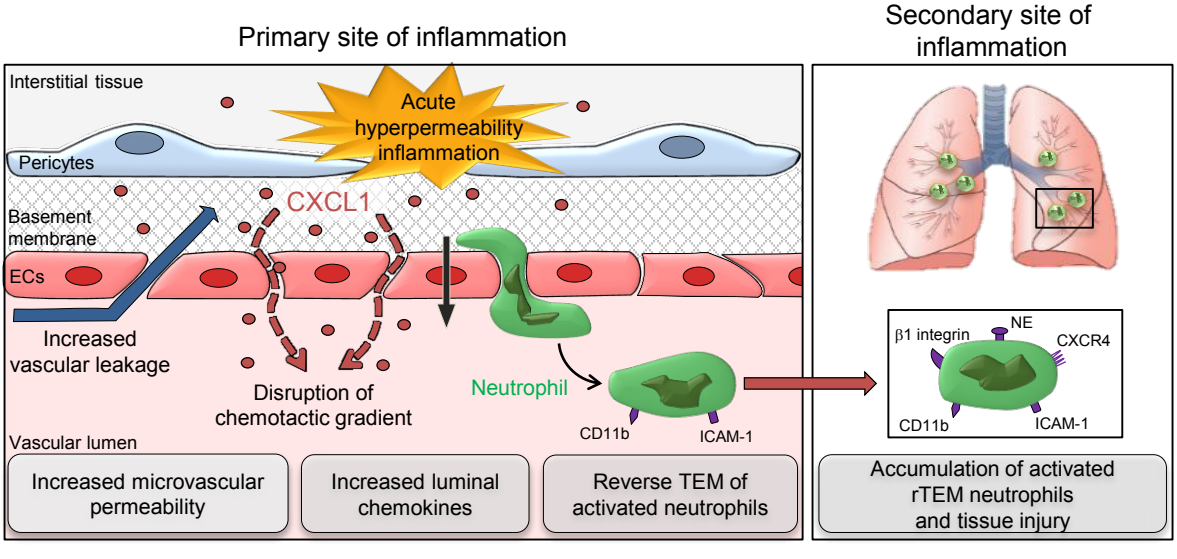
Primary site of inflammation
Secondary site of inflammation
Interstitial tissue
Acute hyperpermeability inflammation
Pericytes
CXCL1
Basement membrane
ECs
Increased vascular leakage
Disruption of chemotactic gradient
Neutrophil
CD11b
ICAM-1
Vascular lumen
β1 integrin
NE
CXCR4
CD11b
ICAM-1
Increased microvascular permeability
Increased luminal chemokines
Reverse TEM of activated neutrophils
Accumulation of activated rTEM neutrophils and tissue injury

Supplemental material

Local microvascular leakage promotes trafficking of activated neutrophils to remote organs

Charlotte Owen-Woods[1], Régis Joulia[1], Anna Barkaway[1], Loic Rolas[1], Bin Ma[1], Astrid Fee Nottebaum[2], Kenton P Arkill[3], Monja Stein[1], Tamara Girbl[1], Matthew Golding[1], David O Bates[3], Dietmar Vestweber[2], Mathieu-Benoit Voisin[1] & Sussan Nourshargh[1,4*]

[1]William Harvey Research Institute, Barts and The London School of Medicine and Dentistry, Queen Mary University of London, Charterhouse Square, London, EC1M 6BQ, UK.

[2]Department of Vascular Cell Biology, Max Planck Institute for Molecular Biomedicine, Röntgenstraße 20, 48149 Münster, Germany.

[3]Division of Cancer and Stem Cells, School of Medicine, University of Nottingham Biodiscovery Institute, University Park, Science Road, Nottingham NG7 2RD UK

[4]Centre for Inflammation and Therapeutic Innovation, Barts and The London School of Medicine and Dentistry, Queen Mary University of London, London, EC1M 6BQ, UK.

C. Owen-Woods and R. Joulia contributed equally to this work.

A. Barkaway and L. Rolas contributed equally to this work.

M-B. Voisin and S. Nourshargh jointly supervised the work.

*Correspondence to Sussan Nourshargh: s.nourshargh@qmul.ac.uk

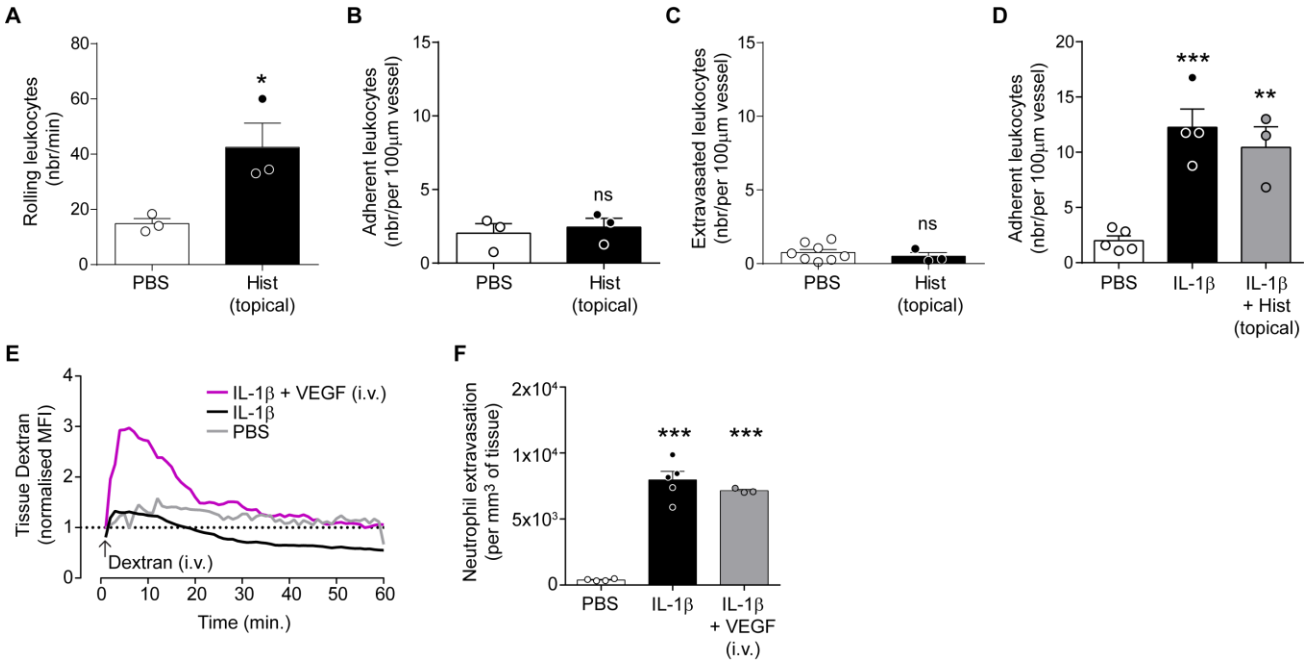

Supplemental Figure 1. Effect of topical histamine and systemic VEGF on neutrophil-vessel wall interactions and microvascular leakage in the cremaster muscle. (**A**-**C**) Cremaster muscles of WT mice were exteriorised, superfused with either histamine (30 μM) or vehicle (PBS) and analysed for neutrophil-vessel wall interactions by brightfield IVM. Number of rolling (**A**, cell number/min, n = 3 mice per group), adherent (**B**, n = 3 mice per group) and extravasated (**C**, n = 3-8 mice per group) leukocytes per 100 μm length of post-capillary venules. (**D**) Effect of topical histamine (30 μM) on leukocyte adhesion in IL-1β-stimulated tissues (n = 3-5 mice per group). (**E** and **F**) *LysM-EGFP-ki* mice, subjected to an i.s. injection of an anti-CD31 mAb to label endothelial cells junctions, were injected with i.s. PBS or IL-1β (50 ng) for 2 h. The mice were then injected i.v. with VEGF (4 μg/mouse) and 75 kDa-TRITC-dextran and neutrophil responses and vascular leakage were analysed by confocal IVM. (**E**) Time-course of dextran leakage into the perivascular region of a selected post-capillary venule (n = 3-5 mice per group). (**F**) Neutrophil extravasation (n = 3-5 mice per group). Data are represented as mean ± SEM (each dot represents one mouse and one independent experiment). Statistically significant differences from PBS are shown by *p<0.05, **p<0.01 ***p<0.001, two-tailed Student's t-test or one-way ANOVA followed by Bonferroni's post hoc test (ns = not significant).

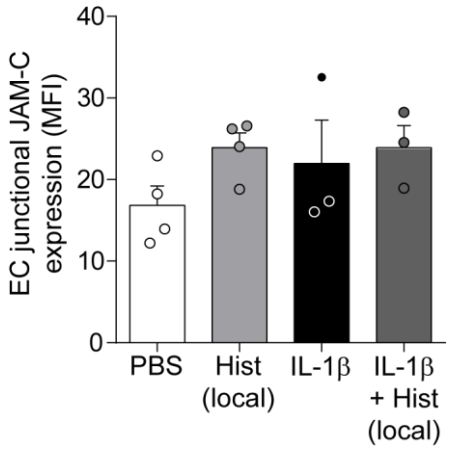

Supplemental Figure 2. Histamine has no impact on endothelial cell junctional JAM-C expression. Cremaster muscles of WT animals were injected with IL-1β or PBS injection (2 h) prior to the local administration of histamine or vehicle for 30 mins. Tissues were then collected, immunostained for JAM-C and the expression of EC junctional JAM-C was quantified by confocal microscopy (n = 3-4 mice per group). Data are represented as mean ± SEM (each dot represents one mouse and one independent experiment). No statistical differences were obtained between any of the groups and PBS as analysed using one-way ANOVA followed by Bonferroni's post hoc test.

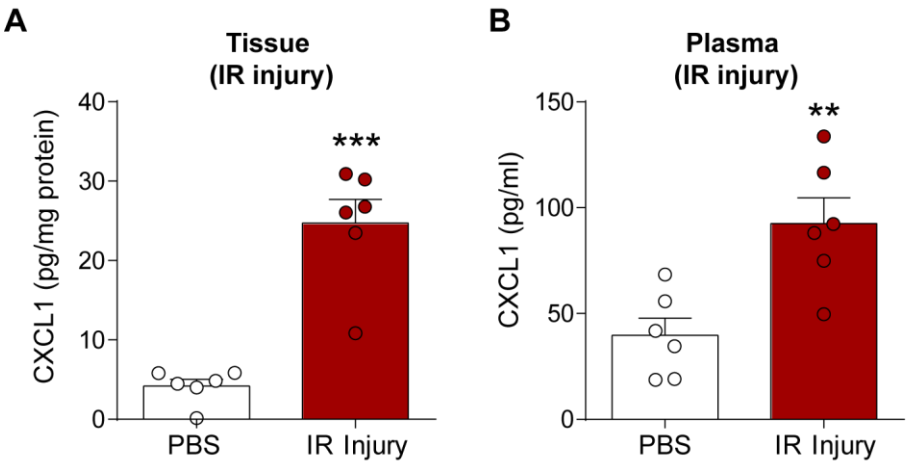

Supplemental Figure 3. Mice subjected to cremasteric IR injury exhibit elevated levels of CXCL1 in tissues and plasma. Cremaster muscles of WT animals were subjected to IR injury (40 min ischemia followed by 30 min reperfusion period). Tissue (**A**) and plasma (**B**) were collected and analysed for CXCL1 levels by ELISA (n = 6 mice per group). Data are represented as mean ± SEM (each dot represents one mouse and one independent experiment). Statistically significant differences from PBS are shown by **p<0.01, ***p<0.001, two-tailed Student's t-test.

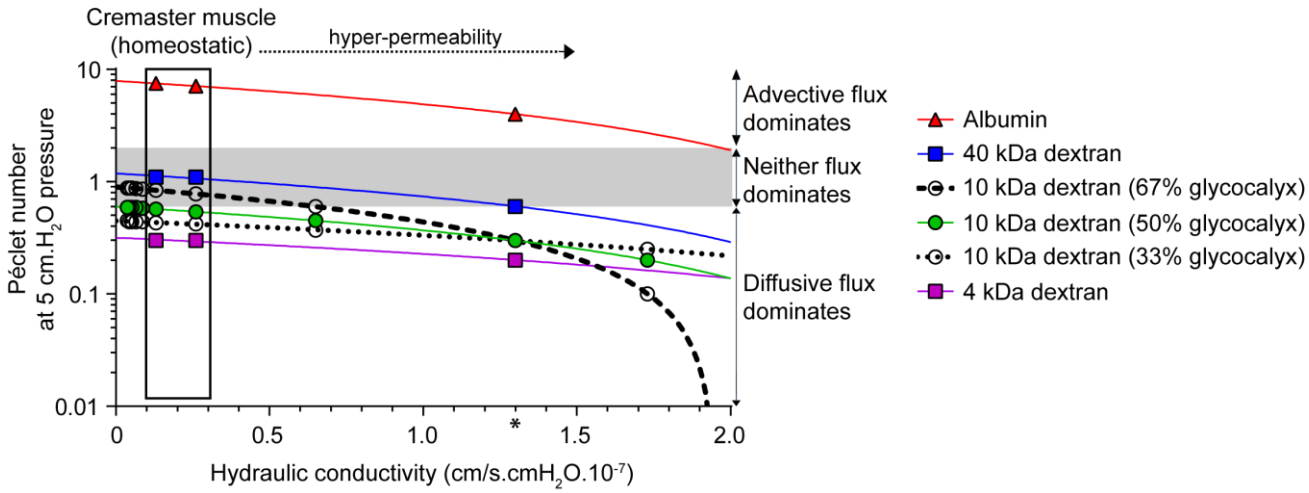

Supplemental Figure 4. Mathematical modelling of molecular flux across cremasteric venules. Estimation of the Péclet number at 5 cm.H_2O net pressure difference for 4 kDa dextran, 40 kDa dextran, albumin and 10 kDa dextran assuming different distributions of resistance across the vessel wall (67% of the resistance across the glycocalyx, 50% across the glycocalyx or 33% across the glycocalyx). The hydraulic conductivity is well characterised from published works as detailed below. The boxed data indicate the hydraulic conductivity in the cremaster muscle microcirculation under homeostatic conditions (0.1-0.3x10^{-7}cm/s.cmH_2O) with the arrow indicating changes in hydraulic conductivity following hyperpermeability.* Indicates typical value for more permeable vessels (e.g. mesenteric capillaries).

Text associated with Supplementary Figure 4

Molecular flux is determined by a combination of diffusive and advective transport. For a macromolecule produced extravascularly to enter the circulation, the diffusive flux from tissue to blood must be high enough to overcome the opposing advective flux. This ratio can be defined by the Péclet number (*Pe*):

$$Pe = \frac{Advective\ Transport\ Rate}{Diffusive\ Transport\ Rate} = \frac{V.L}{D} \qquad \text{EQ. 1}$$

The *advective transport rate* is the hydraulic velocity (*V*) and the *diffusive transport rate* is the diffusion coefficient (*D*) divided by the distance (*L*), determined in the present study by the endothelial intercellular cleft length (1). If the *Pe* is near to 1 then neither fluxes are dominant; if the *Pe* is much greater than 1 then diffusion cannot effectively oppose filtration and the molecule cannot travel against the flow; if *Pe* is much less than 1, then there can be diffusion against the flow of fluid. Although the exact combination and interaction of blood vessel wall molecular and cellular structures on venular wall *Pe* is unknown, particularly during inflammation, a solid understanding of the permeability of the

vessel wall as a whole to both macromolecules and to water (hydraulic conductivity) enables mathematical modelling of molecular flux across cremasteric venular walls. In normal physiology, in continuous vessels such as those in the muscle, the fluid from the pressurised small blood vessel (e.g. postcapillary venules) needs to move through the endothelial cell (EC) glycocalyx, funnelled through the EC intercellular clefts and then further funnelled through the breaks in junctional strands within the EC clefts. In our case *equation 1* can be rewritten for a molecule *i* where $L_p$is the hydraulic conductivity, L_{cleft} the cleft length, D^i_{Cleft} the diffusion coefficient in the cleft, ΔP the net change of pressure, and A_{Open} the area of open cleft available to transport per unit area.

$$Pe^i = \frac{\left[\frac{L_p}{\Delta P.A_{Open}}\right].L_{cleft}}{D^i_{Cleft}} \qquad \text{EQ. 2}$$

Due to the extensive body of research on mesenteric microcirculation permeability the following calculations will be based on mesenteric vessels and then adapted for the cremaster blood vessel where only L_p has been measured.

For every 1 μm^2 of blood vessel surface area there are 0.1 μm of EC intercellular cleft with approximately 0.01 μm of EC open junction for rat mesenteric vessels (2). This equates to 1000 cm of cleft for each cm^2 of venular wall, and 100 cm of open junction. The L_p in the mesenteric vessels is approximately 1.3x10^{-7} cm.s^{-1}.cmH_2O^{-1} and the net driving pressure (Hydrostatic minus Oncotic pressures) would be ~5 cmH_2O (2, 3). If the EC intercellular cleft is 18 nm wide then (maintaining traditional units) the fluid velocity though these slits (V) is calculated to be 3.6x10^{-3} cm/s. D^i_{Cleft} can be calculated through a slit (4, 5):

$$D^i_{Cleft} = D^i_{Free}[1 - 1.004B + 0.418B^3 + 0.210B^4 - 0.1696B^5] \qquad \text{EQ. 3}$$

Where:

$$B = 2a^i/W_{Cleft} \qquad \text{EQ. 4}$$

With a^i as the molecular radius and W_{Cleft} as the cleft width.

D^i_{Cleft} for a 10 kDa dextran in the cleft ($D^{10\ kDa\ dextran}_{Cleft}$) is calculated as 9.3x10^{-7} cm^2.s^{-1}, given an 18 nm slit, assuming free diffusion of 1.1x10^{-6} cm^2.s^{-1} (6) and a Stokes-Einstein radius of 2.3 nm (manufacturer datasheet). The estimated length of the cleft varies from 400 nm to nearer 1000 nm, but assuming a mean length of 700 nm (7) the estimate of $Pe^{10\ kDa\ dextran}$ is 0.3.

For comparison with albumin (using 3.5 nm for the radius (8) and 1.0x10^{-7} cm^2.s^{-1} for free diffusion), $Pe^{Albumin}$ = 4.

Cremaster muscle vessels have not to date been analysed to the same detail but the tissue has previously been estimated to have between 5x and 10x lower L_p (9, 10). These experiments also noted that limiting pore sizes were unlikely to be the reason for the difference between muscle and mesenteric blood vessels, and therefore the available proportion of EC surface area was given as the most likely explanation. Intuitively, if we have only 10% of the available EC cleft area, the resistance is 10-fold higher (L_p is reduced by 10-fold) and would not change the Pe^i. However, the resistance from the endothelial glycocalyx in the mesenteric vessels is similar in magnitude (50% to 150%) to the EC cleft resistance, and therefore contributes between 33 and 67% of the total resistance across the vessel wall. This means that the available area of the cleft would need to be reduced by more than 10-fold (15-fold to 30-fold respectively) to produce a 10-fold reduction in L_p and hence the Pe^i must be greater in the case of cremaster vessels. In Supplemental Figure 4, we model Pe for 10kDa dextran at different hydraulic conductivity and percent contribution of the glycocalyx to endothelial resistance. It can be seen that Pe^{10kDa} rises from 0.3 in the mesentery (L_p ~ 1.3x10^{-7} cm.s^{-1}.cmH$_2$O^{-1}) to between at least 0.4 and likely greater than 0.8 in the cremaster. Therefore the movement of a small molecular weight protein (e.g. a chemokine or 10 kDa dextran) back into the vasculature is likely to be finely balanced under normal conditions as the $Pe^{10kDa\ dextran}$ is approaching unity.

Calculation of Pe^{10kDa} during a hyperpermeability inflammatory response:

The experimental results in this manuscript (see Figure 4) show that topical application of 10 kDa dextran to exteriorised cremaster muscles led to detection of a low level of this molecule in the vasculature under homeostatic conditions. This is in line with the preceding mathematical expectations. Upon addition of histamine, higher levels of 10 kDa dextran were detected in the vasculature, i.e. a decrease in Pe^{10kDa} to substantively less than 1. Since the experiment also involved tracking i.v. injected 75 kDa dextran (used to represent an albumin sized molecule), which was correspondingly increased in the interstitium, these results indicate an increase in hydraulic flux. Clearly, any increase in water flux without a structural change in the cleft region would increase Pe^i rather than decrease it, strongly indicating that in these works a structural change to the vessel had been induced. The principal possibilities are changes to the endothelial glycocalyx or within the EC cleft region.

An endothelial glycocalyx with a 100 nm thick filtration zone exhibiting 9 nm pores with 20 nm spacing has much lower D^i_{Glx}, but as its available surface area is markedly greater covering the whole EC cleft length and the EC cleft entrance (circa 200 nm wide), it may impact the hydraulic velocity within each pore by reducing it (11, 12). Using the above model for diffusion across the EC glycocalyx (using the D^i_{Pore} versions of *Equation 3 and 4*), $Pe^{10\ kDa\ dextran}$ = 0.004 and 0.002 in cremaster and mesenteric vessels respectively ($Pe^{Albumin}$ = 0.1 and 1 respectively) and as such indicates that 10 kDa dextran is completely diffusion dominant in the endothelial glycocalyx. These calculations strongly indicate that

in our experimental model the transport of a 10 kDa molecule from the tissue to the lumen is defined by the EC cleft component of the vessel wall and under increased permeability

If histamine primarily changes the junctional strands in the cremaster exchange vessels, effectively increasing A_{Open} to that of the mesentery (or beyond), $Pe^{10\ kDa\ dextran}$ decreases from near unity to 0.3 (or further). This change results in the 10 kDa dextran diffusion flux to be dominant and hence for the molecule to be far more capable of travelling from the interstitium to the vasculature, even in the presence of the increased hydraulic flux from the vessel to the interstitium.

To comprehend the 75 kDa dextran (representing albumin sized molecules) flux increase one can use the effective solute permeability (P_s). This has been derived numerous times by Curry's group (13) and others, based on calculations by Patlak and colleagues (14)*:*

$$P_s = \left(\frac{e^{Pe}}{e^{Pe}-1}\right)\left[L_p(1-\sigma)\Delta P\right] \qquad \text{EQ. 5}$$

Where the σ is the reflection coefficient, for albumin $\sigma_{Albumin}$ = 0.95 (15). Utilising our parameters for the endothelial cell glycocalyx, the primary albumin resistance, the effective permeability rises from 3.3 x10^{-8} cm.s^{-1} to 5.0 x10^{-8} cm.s^{-1} for the transition from cremaster to mesenteric blood vessels. The tissue albumin concentration would therefore be expected to increase with the expected increase in junctional strand breaks, as observed by the increase in interstitial 75 kDa dextran. Of note is the sensitivity and dependence on Pe: increasing the ΔP by 5 cm.H_2O will make a 1.5-fold change to the mesenteric effective permeability but only 1.05-fold to the cremaster. Our estimate here is low compared to experimental data that ranges from 0.4 x10^{-6} cm.s^{-1} to 3 x10^{-6} cm.s^{-1} but these have various other caveats namely that ΔP was higher, dramatically increasing the sensitive parameter Pe. Further the mathematical derivation, although not phenomenological, is simplistic for several reasons, in particular a perfect membrane of zero thickness.

In conclusion, we have mathematically shown that in normal physiology, the diffusion of a 10 kDa molecule in the cremaster muscle tissue would be expected to be finely regulated. If the breaks in the EC junctional strands are more common, such as when induced by the inflammatory agent histamine that increases vascular permeability, then the tissue concentration of albumin sized molecules will be higher and at the same time, the 10 kDa molecule will be able to enter the vascular lumen. This mathematical prediction fits the experimental observations of the present study.

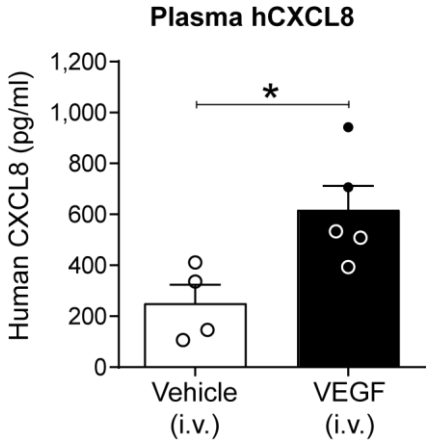

Supplemental Figure 5. VEGF promotes leakage of locally applied human CXCL8 from the tissue into the vascular compartment. Cremaster muscles were injected locally with IL-1β (50 ng) and human CXCL8 (hCXCL8, 500ng) for 1 h, followed by injection (i.v.) of vehicle (control) or VEGF (4 μg) for a further 1 h. hCXCL8 levels in plasma as quantified by ELISA (n = 4-5 mice per group). Data are represented as mean ± SEM (each dot represents one mouse and one independent experiment). Statistically significant difference from vehicle is indicated by *p<0.05, two-tailed Student's t-test.

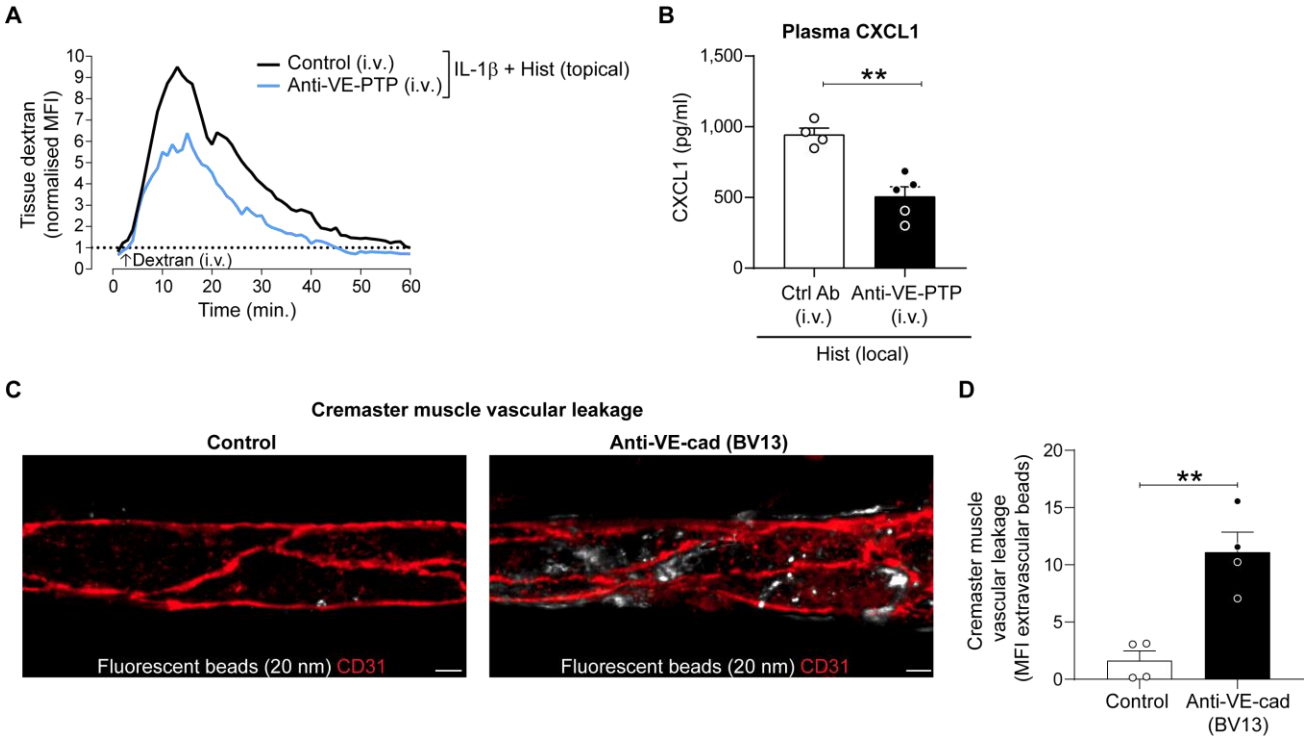

Supplemental Figure 6. Effect of blocking anti-VE-PTP and anti-VE-cadherin antibodies on vascular leakage and chemokine level. **(A-B)** Cremaster muscles of WT mice were stimulated with IL-1β (50 ng for 2 h) followed by topical superfusion of histamine onto exteriorised tissues. Blocking anti-VE-PTP mAb (100-200 μg) was injected i.v. 30 min before exteriorisation of tissues. Control mice received i.v. PBS or control rabbit IgG (no differences were observed between the 2 groups). Fluorescently-labelled anti-CD31 mAb was injected i.s. to visualise endothelial cell junctions and 75 kDa TRITC-dextran was injected i.v. at the beginning of the image acquisition period to visualise and quantify vascular leakage. (**A**) Time-course of dextran accumulation in the perivascular region of selected stimulated post-capillary venules. Tissue dextran accumulation is represented as normalised MFI (n = 3-4 mice per group). (**B**) CXCL1 levels in plasma as quantified by ELISA (n = 4-5 mice per group). (**C**-**D**) Cremaster muscles of WT mice were injected i.s. with a blocking anti-VE-cadherin mAb (BV13, 100 μg) for 4 h. Control mice were injected locally with PBS or anti-CD31 mAb (390, 100 μg) (data pooled as no difference was noted between the groups) for 4 h. Thirty minutes before the end of the in vivo test period, mice were injected i.v. with red-(580/605)-microspheres (20 nm in diameter, 9.1 x 10^{13} beads). Tissues were then collected and immunostained for anti-CD31 (clone 2H8, red) and analysed by confocal microscopy. (**C**) Representative confocal images of post-capillary venular segments from indicated reactions. Scale bars, 5 μm. (**D**) Cremaster muscle vascular leakage as quantified by accumulation (MFI) of extravascular beads (n = 4 mice per group). Statistically significant difference from control is indicated by **p<0.01, two-tailed Student's t-test.

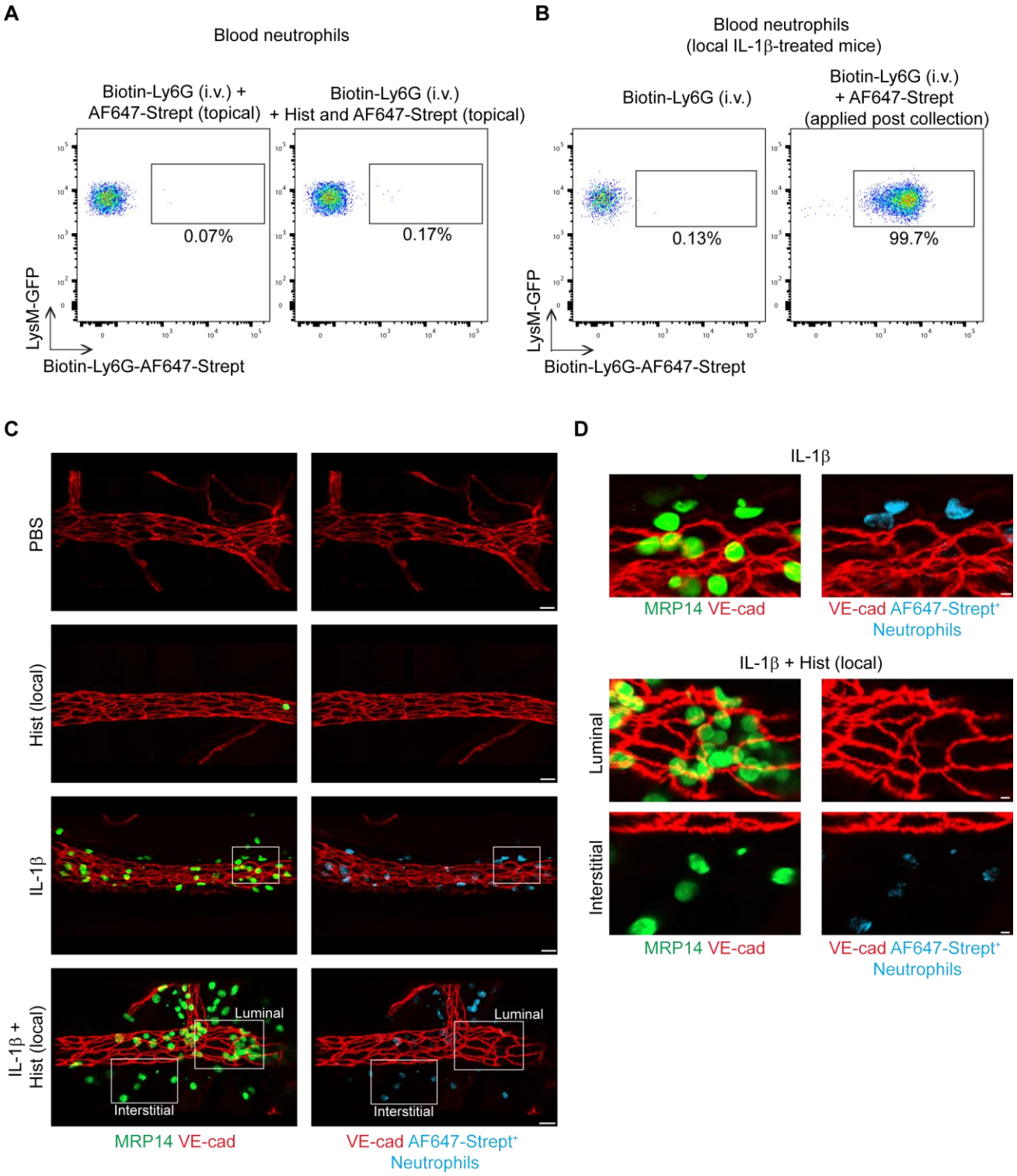

Supplemental Figure 7. Further characterisation of the biotin-Ly6G-AF647-streptavidin in vivo labelling method. (**A**) *LysM-EGFP-ki* mice received an i.v. injection of biotin-Ly6G mAb (2 μg) for 30 min, after which cremaster muscles were exteriorised and superfused with AF647-streptavidin (1 μg/ml) in combination with histamine or vehicle for 2 h. Peripheral blood was collected and analysed by FACS with representative flow cytometry profiles showing the percentage of AF647-Streptavidin^{+} neutrophils presented (representative of 3 independent experiments). (**B**) Cremaster muscles of

LysM-EGFP-ki mice were stimulated with IL-1β (50 ng for 2 h) and the mice were injected i.v. with biotin-anti-Ly6G mAb (2 μg) at t = 90 min. Blood was collected 2 h later and stained with AF647-strept in vitro to analyse the efficiency of biotinylated-anti-Ly6G labelling of circulating neutrophils. Representative flow cytometry profiles showing the percentage of AF647-Streptavidin^{+} neutrophils (representative of 5 independent experiments). (**C** and **D**) Cremaster muscles of WT mice were stimulated locally with IL-1β (50 ng) or PBS for 2 h and the mice were injected i.v. with biotin-anti-Ly6G (2 μg) at t = 90 min. The mice were then injected either with i.s. histamine (200μl of 30 μM solution) or PBS all in conjunction with AF647-streptavidin (400 ng) for 2 h. Tissues were then collected and immunostained for VE-cadherin (red) and MRP14 (neutrophil, green) and analysed by confocal microscopy. (**C**) Representative confocal images of post-capillary venular segments from indicated reactions (left panels) and (**D**) enlarged images of boxed regions where AF647-streptavidin staining is shown within neutrophil isosurface masks (representative of 3 independent experiments). Scale bars, 15 μm (**C**) and 4 μm (**D**).

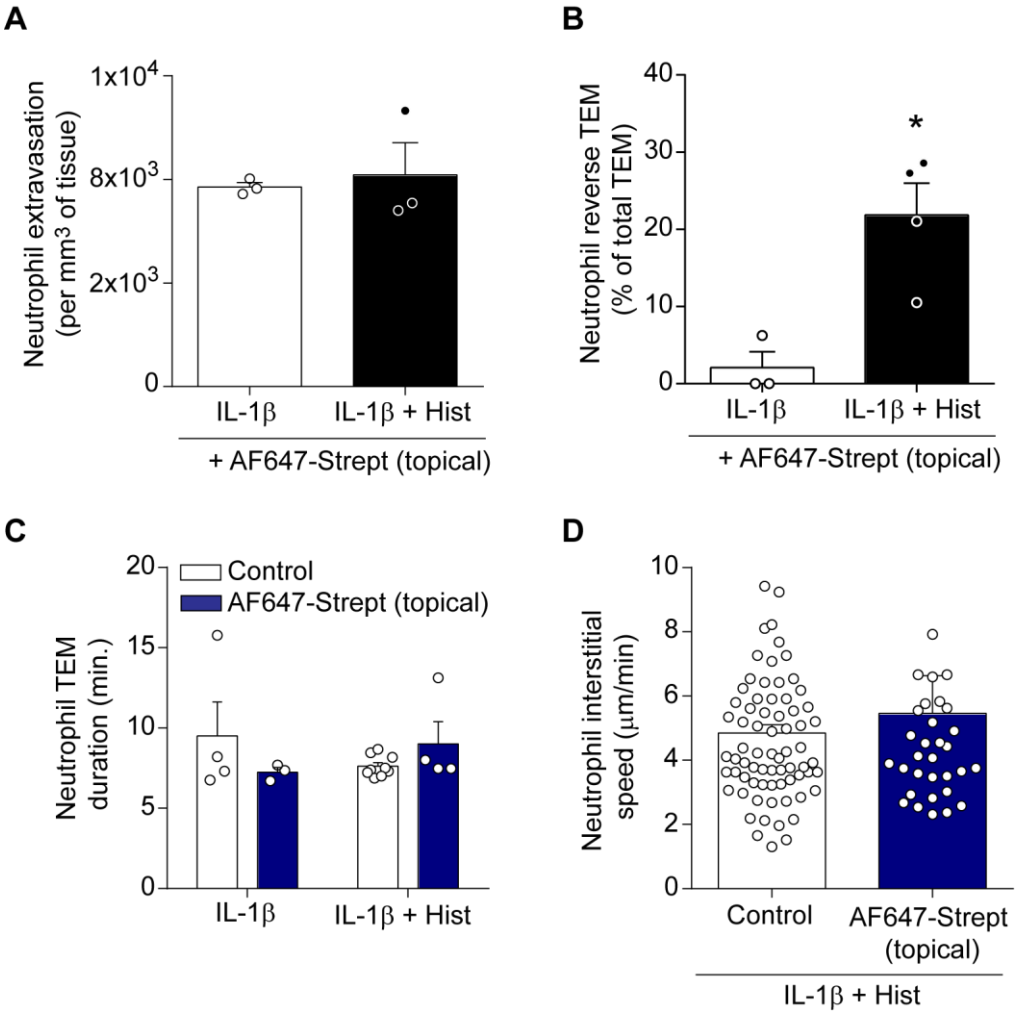

Supplemental Figure 8. The biotin-Ly6G-AF647-streptavidin labelling strategy has no impact on neutrophil motility in vivo. Cremaster muscles of *LysM-EGFP-ki* mice were stimulated locally with IL-1β (50 ng for 1.5 h) followed by an i.v. injection of biotin-anti-Ly6G mAb (2 μg) at t = 90 min. Tissues were then exteriorised and superfused with histamine (30 μM) or vehicle in combination with AF647-streptavidin (1 μg/ml) for 2 h. (**A**) Total neutrophil extravasation (n = 3 mice per group) and (**B**) frequency of neutrophil rTEM (n = 3-4 mice per group) show similar levels compared to reactions quantified in mice not subjected to the labelling strategy (see Figure 2A and D). (**C** and **D**) Mice subjected to the biotin-Ly6G-AF647-streptavidin labelling strategy and unlabelled mice exhibited similar neutrophil TEM duration (**C**, n = 3-9 mice per group) and neutrophil interstitial migration speed (**D**, n = 32-74 neutrophils per group) in cremaster muscles following local stimulation with IL-1β or IL-1β+histamine. Data are represented as mean ± SEM (each point represents one mouse and one independent experiment). Statistically significant differences from IL-1β are shown by *p<0.05, two-tailed Student's t-test.

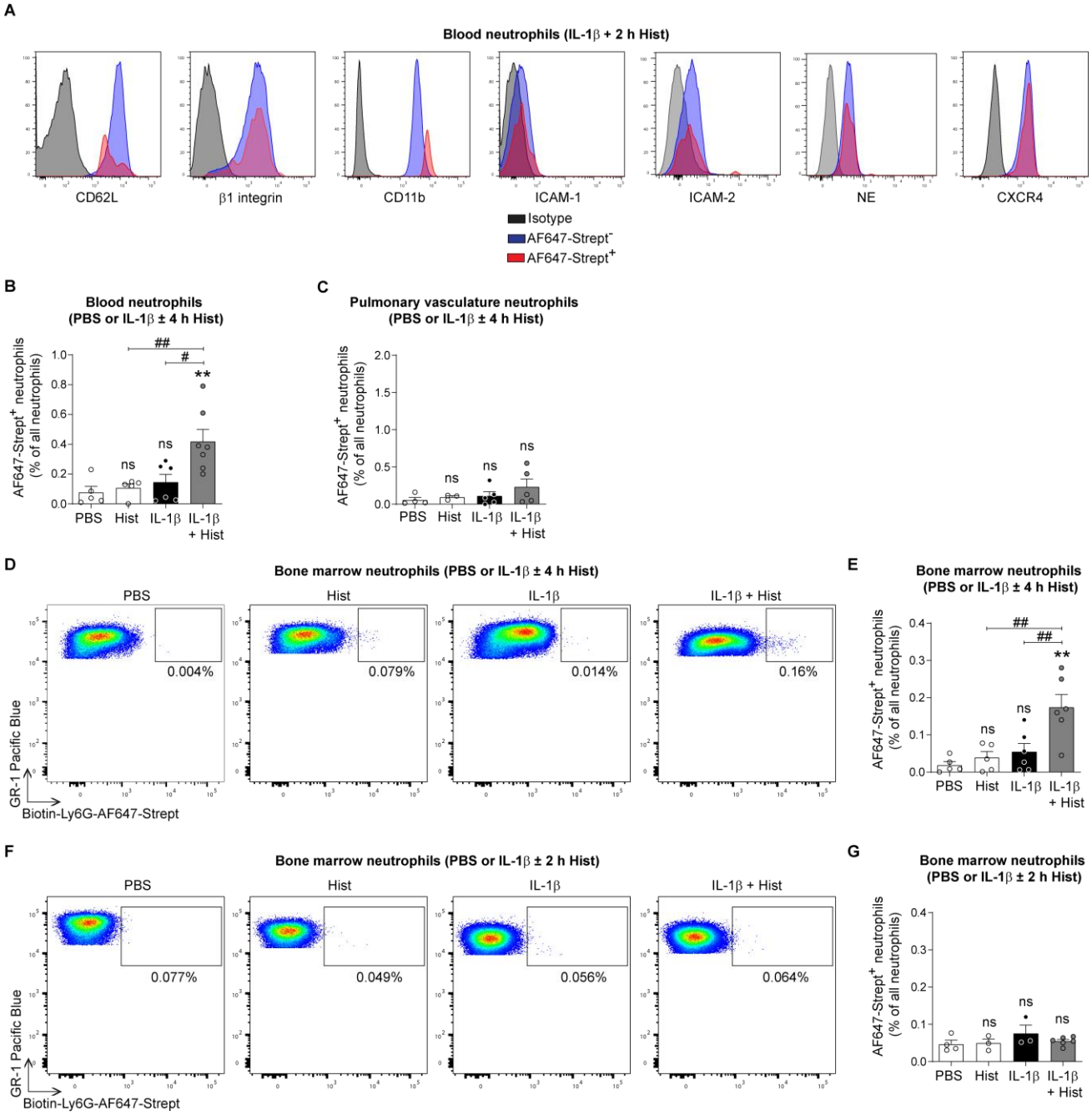

Supplemental Figure 9. In mice subjected to a local hyperpermeability reaction blood AF647-streptavidin$^+$ neutrophils show a distinct activated phenotype and streptavidin$^+$ neutrophils are present in the bone marrow at 4 h but not at 2 h post histamine. Cremaster muscles of WT mice were stimulated with IL-1β (50 ng) or PBS for 2 h followed by an i.s. injection of histamine (200 μl of 30 μM solution) or PBS. Mice were subjected to our biotin-Ly6G-AF647-streptavidin labelling strategy and as such received an i.v. injection of biotin-anti-Ly6G mAb (2 μg) at t = 90 min and were also injected locally with AF647-streptavidin (400 ng) in conjunction with histamine or vehicle for 2-4 h. Peripheral blood, pulmonary vascular washout and bone marrow samples were collected and analysed by flow cytometry. (**A**) Representative flow cytometry histograms of blood neutrophils from

a mouse subjected to cremaster muscle stimulation with IL-1β+histamine and biotin-Ly6G-AF647-streptavidin labelling strategy 2 h post histamine. The sample is assessed for the indicated markers and comparing AF647-Streptavidin^{+} neutrophils with AF647-Streptavidin^{-} neutrophils with relevant isotype control profiles being shown in black (representative of five independent experiments). (**B**) Frequency of blood AF647-Strept^{+} neutrophils (Gr-1^{high}/CD115^{-}) in mice subjected to the indicated cremasteric stimulations (n = 5-7 mice per group). (**C**) Frequency of pulmonary vascular washout AF647-Strept^{+} neutrophils (Gr-1^{high}/CD115^{-}) in mice subjected to the indicated cremasteric stimulations (n = 3-5 mice per group). (**D**) Representative flow cytometry profiles and (**E**) frequency of bone marrow AF647-Strept^{+} neutrophils (Gr-1^{high}/CD115^{-}) in mice subjected to the indicated cremasteric stimulations (n = 5-6 mice per group). (**F**) Representative flow cytometry profiles and (**G**) frequency of bone marrow AF647-Strept^{+} neutrophils (Gr-1^{high}/CD115^{-}) in mice subjected to the indicated cremasteric stimulations (n = 3-6 mice per group). Data are represented as mean ± SEM (each dot represents one mouse and one independent experiment). Statistically significant differences from PBS are shown by **p<0.01 or by indicated comparisons #p<0.05, ##p<0.01, one-way ANOVA followed by Bonferroni's post hoc test (ns = not significant).

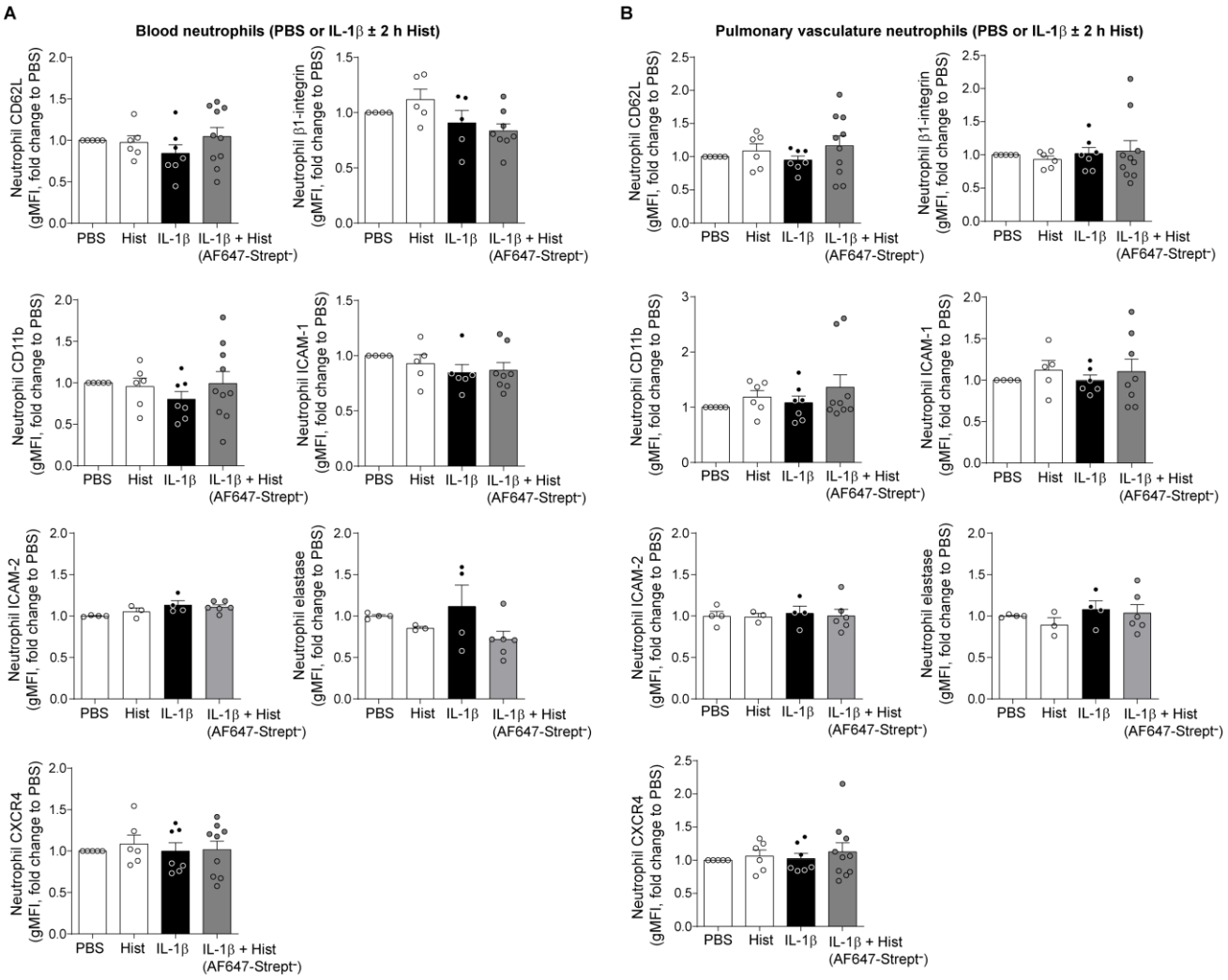

Supplemental Figure 10. Blood and pulmonary vascular washout AF647-Streptavidin⁻ neutrophils show a phenotype similar to that of control cells. WT mice were subjected to cremaster muscle stimulation with IL-1β (50 ng) or PBS for 2 h followed by i.v. injection of biotinylated-anti-Ly6G (2 μg) at t = 90 min. The mice then received an i.s. injection of AF647-Strept (400 ng) co-administered with histamine (200 μl of 30 μM solution) or PBS for 2 hours. Peripheral blood and pulmonary vascular washout were collected and analysed by flow cytometry. (**A** and **B**) The phenotype of AF647-Streptavidin⁻ neutrophils in blood and pulmonary vascular washout samples acquired from mice subjected to cremaster muscle stimulation with IL-1β+histamine and the biotin-Ly6G-AF647-streptavidin labelling strategy was compared to phenotype of neutrophils from unlabelled mice in which the cremaster muscles were stimulated locally with PBS, histamine and IL-1β alone. Results are presented as gMFI fold change compared to the neutrophils of samples acquired from PBS-treated mice (n = 3-10 mice per group). Data are represented as mean ± SEM (each dot represents one mouse and one independent experiment). No statistical differences were obtained between any of the groups and PBS, one-way ANOVA followed by Bonferroni's post hoc test.

References:

1. Michel CC. Starling: the formulation of his hypothesis of microvascular fluid exchange and its significance after 100 years. *Exp Physiol.* 1997;82(1):1-30.
2. Adamson RH, Lenz JF, Zhang X, Adamson GN, Weinbaum S, and Curry FE. Oncotic pressures opposing filtration across non-fenestrated rat microvessels. *J Physiol.* 2004;557(Pt 3):889-907.
3. Betteridge KB, et al. Sialic acids regulate microvessel permeability, revealed by novel in vivo studies of endothelial glycocalyx structure and function. *J Physiol.* 2017;595(15):5015-35.
4. Michel CC, Curry FE. Microvascular permeability. *Physiol Rev.* 1999;79(3):703-61.
5. Weinbaum S, Tsay R, and Curry FE. A three-dimensional junction-pore-matrix model for capillary permeability. *Microvasc Res.* 1992;44(1):85-111.
6. Kvist P, Schuster E, Lorén N, and Rasmuson A. Using fluorescent probes and FRAP to investigate macromolecule diffusion in steam-exploded wood. *Wood Sci Technol.* 2018;52(5):1395-410.
7. Li G, Yuan W, and Fu BM. A model for the blood-brain barrier permeability to water and small solutes. *J Biomech.* 2010;43(11):2133-40.
8. Armstrong JK, Wenby RB, Meiselman HJ, and Fisher TC. The hydrodynamic radii of macromolecules and their effect on red blood cell aggregation. *Biophys J.* 2004;87(6):4259-70.
9. Curry FE, Frokjaer-Jensen J. Water flow across the walls of single muscle capillaries in the frog, Rana pipiens. *J Physiol.* 1984;350:293-307.
10. Smaje L, Zweifach BW, and Intaglietta M. Micropressures and capillary filtration coefficients in single vessels of the cremaster muscle of the rat. *Microvasc Res.* 1970;2(1):96-110.
11. Arkill KP, et al. Similar endothelial glycocalyx structures in microvessels from a range of mammalian tissues: evidence for a common filtering mechanism? *Biophys J.* 2011;101(5):1046-56.
12. Squire JM, Chew M, Nneji G, Neal C, Barry J, and Michel C. Quasi-periodic substructure in the microvessel endothelial glycocalyx: a possible explanation for molecular filtering? *J Struct Biol.* 2001;136(3):239-55.
13. Huxley VH, Curry FE, and Adamson RH. Quantitative fluorescence microscopy on single capillaries: alpha-lactalbumin transport. *Am J Physiol.* 1987;252(1 Pt 2):H188-97.
14. Patlak CS, Goldstein DA, and Hoffman JF. The flow of solute and solvent across a two-membrane system. *J Theor Biol.* 1963;5(3):426-42.
15. Michel CC, Kendall S. Differing effects of histamine and serotonin on microvascular permeability in anaesthetized rats. *J Physiol.* 1997;501(Pt 3):657-62.

Supplemental movie legends

Supplemental movie 1 (related to Figure 1A). Microvascular leakage and neutrophil TEM in an IR-stimulated cremaster muscle. The movie captures a post-capillary venule after 40 min of ischemia in a *LysM-EGFP-ki* mouse. EC junctions were labelled in vivo with an AF647-anti-CD31 mAb (red). 75 kDa TRITC-dextran was injected i.v. 2 min after the beginning of the acquisition. The video shows luminal views of GFP^{bright} neutrophils (green) interacting with ECs (left panel) and trafficking of vascular dextran (blue pseudocolor intensity; right panel). The movie illustrates the development of an inflammatory response during IR with neutrophils breaching EC junctions and the occurrence of rapid and localised areas of intravascular dextran leakage (exemplified by boxed regions). Dextran signal was smoothed using a Gaussian filter for clarity using Imaris software. Still images of this video are shown in Figure 1A.

Supplemental movie 2 (related to Figure 1D). Neutrophil normal TEM in an IR-stimulated cremaster muscle. The confocal IVM movie shows a cremaster muscle post-capillary venule of a *LysM-EGFP-ki* mouse in which the TEM of a GFP^{bright} neutrophil is tracked during reperfusion phase of an IR reaction. EC junctions were labelled in vivo with an AF647-anti-CD31 mAb (red). In addition, 75 kDa TRITC-dextran was injected i.v. 2 min after the beginning of the acquisition; the signal was removed from the video for clarity. The video shows luminal views and the cross section of a selected neutrophil in high optical magnification undergoing TEM. The neutrophil was isolated from the inflammatory response for improved clarity by creating an isosurface using Imaris software. Still images of this video are shown in Figure 1D.

Supplemental movie 3 (related to Figure 1D). Neutrophil reverse TEM in an IR-stimulated cremaster muscle. The confocal IVM movie shows an IR injury response of a cremaster muscle post-capillary venule in a *LysM-EGFP-ki* mouse. The movie tracks GFP^{bright} neutrophils (green) during the reperfusion phase with EC junctions being labelled in vivo with an AF647-anti-CD31 mAb (red). The video shows luminal views and the cross section of a selected neutrophil. The neutrophil that is initially on the luminal side of the endothelium, transmigrates into the sub-EC space and subsequently migrates through EC junctions back into the vascular lumen, i.e. exhibits reverse TEM and re-enters the blood circulation. The neutrophil was isolated from the inflammatory response by creating an isosurface using Imaris software for clarity. Still images of this video are shown in Figure 1D.

Supplemental movie 4 (related to Figure 2B). Microvascular leakage and neutrophil reverse TEM as induced by IL-1β and topical histamine. The movie captures a cremaster muscle post-capillary venule in a *LysM-EGFP-ki* mouse in which GFP^{bright} neutrophils (green) are tracked post local treatment with IL-1β and topical histamine (30 μM). EC junctions were labelled in vivo with an AF647-anti-CD31 mAb (red). In addition, 75 kDa TRITC-dextran (blue pseudocolor intensity) was injected i.v. 3 min after the beginning of the image acquisition**.** The first part of the video shows the development of an inflammatory response illustrating luminal neutrophil-EC interactions. In addition, the video shows dextran extravasation after the topical application of histamine. The second part of the video shows high magnification images of a selected neutrophil within the same vessel segment undergoing reverse TEM. The neutrophil which is already in the sub-EC space migrates through EC junction in an abluminal-to-luminal direction. Dextran signal was smoothed using a Gaussian filter and the neutrophil was isolated from the inflammatory response by creating an isosurface using Imaris software for clarity. Still images of this video are shown in Figure 2B.

Supplemental movie 5 (related to Figure 4E). Interstitial 10 kDa AF488-dextran traffics through leaky venules into the blood stream. The movie shows a post-capillary venule in a WT mouse locally stimulated with IL-1β. EC junctions were labelled in vivo with an AF647-anti-CD31 mAb (blue). 75 kDa TRITC-dextran (red) was injected i.v. 2 min and 10 kDa AF488-dextran (green) was superfused 7 min after the beginning of the image acquisition. At t = 17 min, 10 kDa AF488-dextran was removed from the superfusate and replaced by Tyrode's solution containing 30 μM histamine. For clarity, EC junctions and 75 kDa TRITC-dextran signals are shown on the left side and during the first part of the video. Similarly, EC junctions and 10 kDa AF488-dextran are shown on the right side and during the second part of the video. Collectively the movie shows that immediately after topical histamine the intravascular 75 kDa TRITC-dextran rapidly leaks into the perivascular space (indicative of enhanced vascular leakage) while free flowing interstitial 10 kDa AF488-dextran disappears from the tissue compartment (or is captured by perivascular cells). Dextran signals were smoothed using a Gaussian filter for clarity using Imaris software. Still images of this video are shown in Figure 4E.

Supplemental movie 6 (related to Figure 7C). Topical AF647-streptavidin efficiently labels rTEM neutrophils. *LysM-EGFP-ki* mice were stimulated with IL-1β (50 ng for 2 h) followed by an i.v. injection of biotin-anti-Ly6G mAb (2 μg) to label blood neutrophils at t = 90 min. Tissues were then exteriorised and superfused with histamine (30 μM) in conjunction with AF647-streptavidin (1 μg/ml) for 2 h. The movie tracks GFP^{bright} neutrophils (blue) during the vascular leakage phase induced by histamine with EC junctions being labelled in vivo with an AF555-anti-CD31 mAb (green). The tracked

neutrophil that is initially on the luminal side of the endothelium, initiates TEM and during this process its leading body within the sub-EC space rapidly becomes AF647-Strept^{+}. When the neutrophil reverse migrates through EC junctions and re-enters the vascular lumen, AF647-streptavidin quickly redistributes around the surface of the cell and hence the rTEM neutrophil is effectively labelled as AF647-Strept^{+}. The neutrophil was isolated from the inflammatory response by creating an isosurface using Imaris software for clarity. Still images of this video are shown in Figure 7C.